



Article

PSI Photoinhibition and Changing CO₂ Levels Initiate Retrograde Signals to Modify Nuclear Gene Expression

Mehmet Kılıç , Ville Käpylä, Peter J. Gollan , Eva-Mari Aro and Eevi Rintamäki *

Molecular Plant Biology, Department of Life Technologies, University of Turku, 20014 Turku, Finland; mehmet.kilic@utu.fi (M.K.); ville.kapyla@utu.fi (V.K.); peter.gollan@utu.fi (P.J.G.); evaaro@utu.fi (E.-M.A.)

* Correspondence: evirin@utu.fi

Abstract: Photosystem I (PSI) is a critical component of the photosynthetic machinery in plants. Under conditions of environmental stress, PSI becomes photoinhibited, leading to a redox imbalance in the chloroplast. PSI photoinhibition is caused by an increase in electron pressure within PSI, which damages the iron–sulfur clusters. In this study, we investigated the susceptibility of PSI to photoinhibition in plants at different concentrations of CO₂, followed by global gene expression analyses of the differentially treated plants. PSI photoinhibition was induced using a specific illumination protocol that inhibited PSI with minimal effects on PSII. Unexpectedly, the varying CO₂ levels combined with the PSI-PI treatment neither increased nor decreased the likelihood of PSI photodamage. All PSI photoinhibition treatments, independent of CO₂ levels, upregulated genes generally involved in plant responses to excess iron and downregulated genes involved in iron deficiency. PSI photoinhibition also induced genes encoding photosynthetic proteins that act as electron acceptors from PSI. We propose that PSI photoinhibition causes a release of iron from damaged iron–sulfur clusters, which initiates a retrograde signal from the chloroplast to the nucleus to modify gene expression. In addition, the deprivation of CO₂ from the air initiated a signal that induced flavonoid biosynthesis genes, probably via jasmonate production.

Keywords: chloroplast retrograde signaling; FeS clusters; photoinhibition; photosystem I; redox imbalance



Citation: Kılıç, M.; Käpylä, V.; Gollan, P.J.; Aro, E.-M.; Rintamäki, E. PSI Photoinhibition and Changing CO₂ Levels Initiate Retrograde Signals to Modify Nuclear Gene Expression. *Antioxidants* **2023**, *12*, 1902. <https://doi.org/10.3390/antiox12111902>

Academic Editor: Christophe Brunet

Received: 21 September 2023

Revised: 10 October 2023

Accepted: 16 October 2023

Published: 24 October 2023



Copyright: © 2023 by the authors. Licensee MDPI, Basel, Switzerland. This article is an open access article distributed under the terms and conditions of the Creative Commons Attribution (CC BY) license (<https://creativecommons.org/licenses/by/4.0/>).

1. Introduction

Photosynthesis uses solar energy to split water molecules in photosystem (PS) II on the lumenal side of the thylakoid membrane and transfers the electrons through the photosynthetic electron transport chain (PETC) to PSI, which reduces NADP⁺ in chloroplast stroma. Electron transport through the PETC simultaneously pumps protons from the stroma into the thylakoid lumen, which activates ATP synthesis by ATP synthase. ATP and NADPH energize CO₂ fixation in the Calvin–Benson–Bassham (CBB) cycle and other metabolic pathways in the chloroplast. During photosynthetic electron transport, reactive oxygen species (ROS) are generated as by-products in PSII and PSI, especially under stress conditions. ROS, if not properly scavenged, can cause oxidative stress, but they also operate as retrograde signals that help plants to acclimate to stressful conditions [1,2]. Alternatively, electrons can also be redirected from PSI back to the PETC via cyclic electron flow (CEF), thereby strengthening the photosynthetic control mechanism and balancing the electron transport process.

Both photosystems are prone to photoinhibition, which can induce damage to the PS reaction centers, particularly in changing environmental conditions of their natural growth habitats. Under stress conditions, photoinhibition mostly impacts PSII, which in turn protects PSI from photodamage [3,4]. In chilling-sensitive plants such as cucumber, PSI photoinhibition (PSI-PI) occurs under illumination at low (4 °C) temperatures [5,6]. The degradation and replacement of the damaged PSI complex with newly synthesized

PSI subunits take considerably longer than the repair of damaged PSII, which has its own dedicated repair mechanisms [3,6,7].

Upon illumination, the charge separation in PSI produces an oxidized electron donor, $P700^+$, and a reduced primary electron acceptor, A_0^- , a chlorophyll a molecule that further transfers the electron to phylloquinone (A_1). To compensate for the loss of an electron, the oxidized $P700^+$ is reduced by plastocyanin (PC) on the lumenal side of the thylakoid membrane. A_1 donates the electron to an iron–sulfur (FeS) cluster, FeS_X , and then via FeS_A and FeS_B to stromal soluble ferredoxin (FD). The FeS clusters of PSI are susceptible to damage by reactive oxygen species (ROS) under stress conditions, caused by a lack of sufficient oxidized stromal electron acceptors upon excessive electron arrival from PSII [8,9]. The donation of electrons from over-reduced PSI to O_2 leads to the production of superoxide ($O_2^{\bullet-}$), which is converted into hydrogen peroxide (H_2O_2). H_2O_2 reacts with FeS clusters, leading to PSI photoinhibition and the formation of hydroxyl radicals through the Fenton reaction [10–12]. Hydroxyl-radical-induced damage has been shown to target the PSI core subunits PsaA and PsaB [9,13,14].

Irreversible PSI damage and a long repair process impact the redox state in chloroplasts, which may initiate a signaling cascade from the chloroplast to the nucleus to modulate gene expression for the protection and readjustment of chloroplast functions. In addition to extensively investigated chloroplast retrograde signaling during photomorphogenic development [15,16], several other chloroplast signaling pathways initiated by ROS, hormones, sugars, or redox imbalances within PETC and its electron sinks have been shown to operate in chloroplasts and relay information to adjust nuclear gene expression and initiate stress responses in plant leaves [17,18]. Besides ROS, redox imbalances in chloroplasts also lead to the generation of reactive electrophile species (RES), which can initiate signals via reactions with cellular proteins and lipids. Photosynthetic light reactions generate singlet oxygen (1O_2), mainly in PSII, and PSI produces $O_2^{\bullet-}$, which can be converted to H_2O_2 with a longer lifetime. In addition to the generation of ROS in photosynthetic light reactions, photorespiration also produces H_2O_2 in peroxisomes, and this reaction is enhanced by decreasing the CO_2 concentration. The production of ROS by the PETC can trigger the synthesis of oxylipins, such as 12-oxo-phytodienoic acid (OPDA) and jasmonic acid (JA). OPDA is a type of RES and can oxidize lipids and proteins due to its reactive cyclopentane ring [19,20]. OPDA is detoxified by glutathionylation but can also be enzymatically converted to JA [21]. OPDA and JA have been shown to initiate signals that modify gene expression in the nucleus [22,23].

The likelihood of PSI photoinhibition can be mitigated by several mechanisms that reduce electron pressure within PSI, either by downregulating electron flow to the donor side of PSI or by increasing the capacity on the acceptor side. Such protective mechanisms in the former case include PSII photoinhibition, non-photochemical quenching (NPQ), and the photosynthetic control of electron transport through cytochrome b6f, while the latter includes CEF, the water–water cycle, the CBB cycle, and photorespiration [8,24], with the CBB cycle being the major sink for electrons from PSI. Therefore, we hypothesized that increasing the CO_2 concentration upon PSI photoinhibition (PSI-PI) treatment could protect PSI against damage by providing more electron sinks, whilst decreasing the CO_2 concentration would expose PSI to greater damage and originate a retrograde signal from chloroplasts to the nucleus to alleviate the consequences of PSI damage. To this end, we tested whether the putative production of ROS on the PSI acceptor side, oxidized lipids via the production of OPDA and JA, or damage to the FeS clusters in PSI could initiate a signaling cascade to change nuclear gene expression toward the photoprotection of PSI.

2. Materials and Methods

2.1. Growth Conditions and Light Treatments

Wild-type *Arabidopsis thaliana* (Columbia ecotype) was grown in a mixture of soil/vermiculite (2:1) under an 8 h photoperiod at $100 \mu\text{mol photons m}^{-2} \text{s}^{-1}$ (GL) with POWERSTAR HQI-T 400 W/D metal halide lamps (OSRAM GmbH, Munich Germany) as the light

source at 23 °C and 60% relative humidity. Six-week-old plants were used for experiments. Plants were moved from growth conditions to the treatment chamber at 11 a.m. and were allowed to stabilize for 10 min in chamber conditions prior to the specific PSI-PI light treatment. A single PSI-PI treatment cycle [25] consisted of 30 s of growth light followed by three repeated cycles of 5 s of red light (660 nm , $35 \mu\text{mol photons m}^{-2} \text{ s}^{-1}$) and 1 s of intense white light ($1000 \mu\text{mol photons m}^{-2} \text{ s}^{-1}$) using programmable LED lamps (Heliospectra, Göteborg, Sweden). The PSI-PI cycles were repeated for 3 h. Control plants were treated with GL intensity. Plants were subjected to PSI-PI treatment or to GL at CO₂ concentrations of 0 ppm, 100 ppm, 400 ppm, and 1000 ppm using an air-tight chamber (Figure 1).

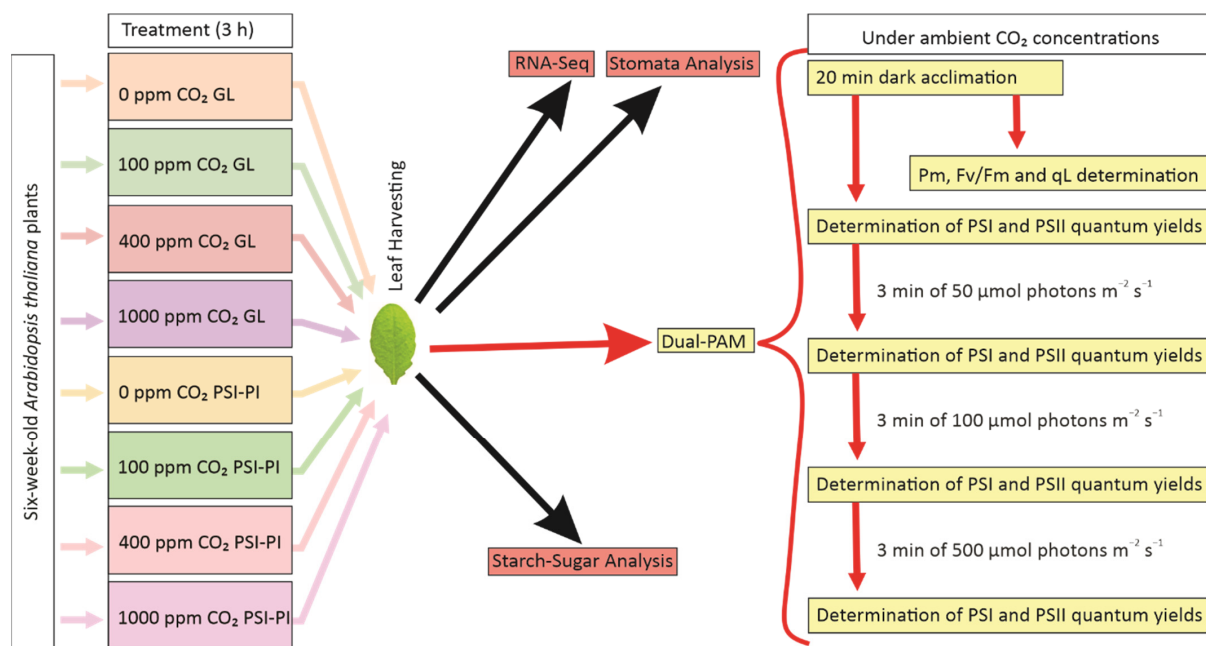


Figure 1. Experimental design to investigate the effects of PSI photoinhibition treatment on photosynthetic activity and gene expression at different CO₂ concentrations. Six-week-old *Arabidopsis thaliana* plants were treated for 3 h with PSI photoinhibition (PSI-PI) treatment or with growth light (GL) as a control. The leaves of treated plants were harvested for the analyses of photosynthesis (Dual-PAM), gene expression (RNA-Seq), stomatal function, and sugar/starch content. Dual-PAM measurements were carried out at atmospheric CO₂. After dark acclimation for 20 min, the maximum oxidation of P700 (Pm), the photochemical efficiency of PSII (Fv/Fm), and a fraction of functional PSII centers (qL) were measured in 8 leaves. For the determination of quantum yields of photosystems, the leaves were subsequently illuminated at 25, 50, 100, and 500 $\mu\text{mol photons m}^{-2} \text{ s}^{-1}$, each for 3 min.

2.2. Biophysical Measurements

The Dual-PAM-100 (Walz, Effeltrich, Germany) was used to simultaneously measure the chlorophyll a fluorescence and P700-oxidation signal in detached leaves. Before the measurements, the leaves were incubated in darkness for 20 min. The photochemical efficiency of PSII was recorded as a ratio of variable to maximum fluorescence (Fv/Fm). The maximum oxidation of P700 (Pm) was determined after far-red illumination, followed by a saturating pulse. The fraction of open PSII reaction centers in the lake model (qL) was determined following the methodology outlined by Kramer et al. [26]. The calculation involved estimating the minimum fluorescence in light (F0') using the approach proposed by Oxborough et al. [27]. Statistical significance between different samples was tested using a one-way ANOVA with the post hoc Tukey HSD Calculator (https://astatsa.com/OneWay_Anova_with_TukeyHSD/ accessed on 1 November 2022).

For the determination of the quantum yields of photosystems, the leaves were subsequently illuminated at 25, 50, 100, and 500 $\mu\text{mol photons m}^{-2} \text{ s}^{-1}$ for 3 min before the measurements. The yield of functional PSI centers (Y(I)), the yield of the donor-side

limitation (Y(ND)), and the yield of the acceptor-side limitation (Y(NA)) were calculated by normalizing the Pm for each leaf sample using the average Pm value of the GL samples at 400 ppm CO₂ as a reference Pm (PmR). This normalization procedure effectively eliminates the contribution of damaged PSI reaction centers to Y(I), Y(ND), and Y(NA) [28]. The photochemical quantum yield of PSII (Y(II)), the yield of non-photochemical quenching (Y(NPQ)), and the yield of nonregulated energy dissipation (Y(NO)) were calculated following the methodology proposed by Genty et al. [29].

2.3. RNA Isolation, Sequencing, and Data Analyses

The seventh plant leaf was used for RNA extraction with four biological replicates. RNA was isolated using an innuPREP plant RNA isolation kit (Analytik Jena) according to the manufacturer's instructions. The total RNA was then converted to cDNA with the Biorad iScript cDNA Synthesis Kit according to their instructions. The cDNA samples were sent to the BGI Europe Genomic Center (Copenhagen, Denmark) for sequencing.

The raw sequence reads from each replicate were quantified with Salmon (v0.12) [30] software using *Arabidopsis thaliana* genome assembly TAIR10 cDNA sequences for the index. The transcript-level estimates from the Salmon software output were imported using 'tximport' R package (v3.16) and subsequently aggregated to the gene level [31]. Analyses of differential gene expression were carried out with the Bioconductor DESeq2 R package (v3.16) [32]. Genes with combined read counts lower than 10 were eliminated before differential expression analyses were performed. Genes with $-1 \geq \log_2(\text{FC}) \geq 1$ were selected for gene enrichment analyses. Gene enrichment analysis was performed with <http://geneontology.org/> (accessed on 10 January 2023) software [33–35]. The gene lists for heatmaps were compiled manually based on GO terms or the published literature, and the heatmaps were created using the Pheatmap R package (v1.0.12).

2.4. Sugars and Starch Analysis

The eighth leaves from the *Arabidopsis thaliana* plants were harvested, flash-frozen in liquid N₂, and then ground with a bead beater for measurements of starch, sucrose, D-fructose, and D-glucose. Measurements were carried out with Megazyme total starch and Sucrose/D-Fructose/D-Glucose assay kits (K-SUFRG; Megazyme, Wicklow, Ireland) according to the manufacturer's instructions. Statistical significance between different samples was tested using a one-way ANOVA with the post hoc Tukey HSD Calculator (https://astatsa.com/OneWay_Anova_with_TukeyHSD/ accessed on 1 May 2023).

2.5. Stomatal Aperture Measurement

Four leaves per PSI-PI treatment were detached from the plants and immediately imprinted on Affinis Precious Polyvinylsiloxane resin (Coltene, Cuyahoga Falls, OH, USA). The resulting negative imprints of the bottom side of each leaf were coated with quick-dry nail polish, and the thin transparent layers were observed under a microscope. From each leaf, approximately 40 stomata were imaged at 40× magnification using the EVOS M5000 Imaging System (Thermo Fischer Scientific, Waltham, MA, United States). The width and length of stomatal apertures were measured using ImageJ software (Fiji, v2.9.0), and the stomatal aperture index (SAI) was calculated as width per length.

3. Results

3.1. Susceptibility of PSI to Specific Photoinhibition Treatment Is Almost Independent of CO₂ Concentration

As summarized in Figure 1, plants were exposed to either the PSI-PI treatment, which induces PSI photoinhibition, or to GL for three hours at a CO₂ concentration of 0 ppm, 100 ppm (low), 400 ppm (atmospheric), or 1000 ppm (high). After the treatments, leaves were harvested for the analyses of gene expression (RNA-Seq), sugar quantity, and stomatal aperture, as well as for the determination of photosynthetic parameters after 20 min of dark incubation. Measurements of PSII fluorescence parameters and the maximum oxidation of

PSI were recorded at atmospheric CO₂. The PSI-PI treatment reduced the PSI oxidation capacity by about 50% at all CO₂ concentrations tested (Figure 2). Interestingly, the absence of CO₂ did not exacerbate PSI photoinhibition, and 1000 ppm CO₂ concentration did not protect PSI from photoinhibition (Figure 2A). The PSI-PI treatment caused only a slight decrease in the Fv/Fm of PSII (Figure 2B) and an approximately 20% decrease in qL (Figure 2C) at all CO₂ conditions.

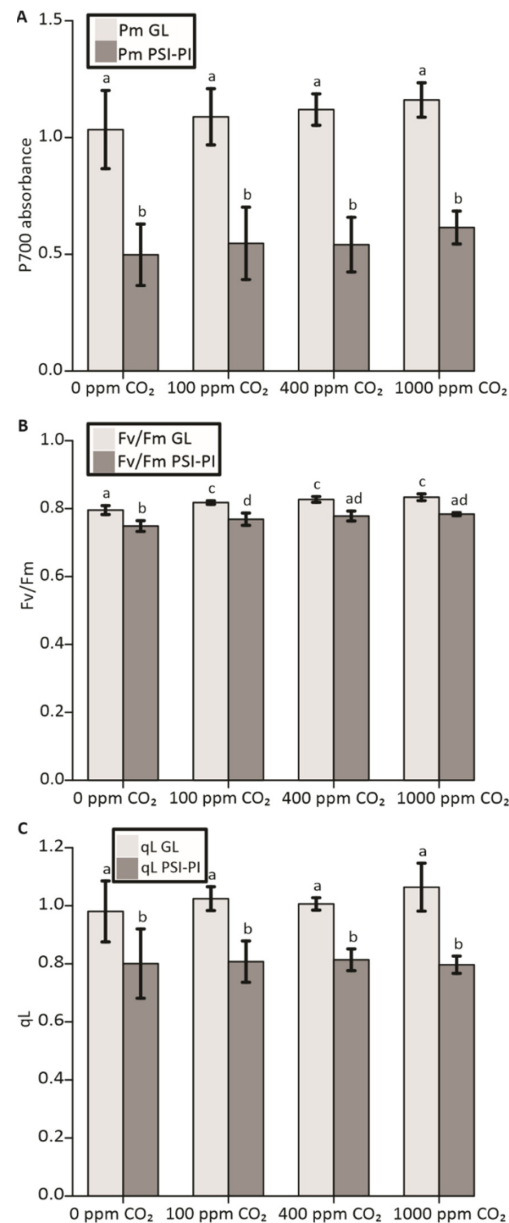


Figure 2. Photosynthetic parameters in *Arabidopsis* plants treated with growth light (GL; light gray) or with PSI photoinhibition (PSI-PI; dark gray) treatment at various CO₂ concentrations. Light treatments were carried out for three hours at CO₂ concentrations of 0 ppm, 100 ppm, 400 ppm, and 1000 ppm. Principal photosynthetic parameters were measured with the Dual-PAM 100 (WALZ) on 8 leaves after dark adaptation for 20 min. (A) Maximum oxidation of P700 (Pm). (B) Maximum quantum efficiency of PSII photochemistry (Fv/Fm). (C) Fraction of functional PSII centers in dark-acclimated samples (qL). Error bars represent standard deviations, and the letters indicate significant differences between the treatments (ANOVA, Tukey HSD, $p < 0.05$).

Plants exposed to either the PSI-PI or GL treatment at different CO₂ concentrations were subjected to measurements of the quantum yields of PSI and PSII at different light in-

tensities (Figure 3). The quantum yields of PSI, indicative of PSI photochemistry ($Y(I)$), were calculated for the remaining functional PSI centers after the PSI-PI treatment (see Materials and Methods). The quantum yields of functional PSI centers were approximately 50% lower in PSI-PI-treated plants measured at light intensities of 0, 50, and 100 $\mu\text{mol photons m}^{-2} \text{s}^{-1}$ in comparison to control plants without PSI-PI treatment (Figure 3A). Under high light, $Y(I)$ of PSI-PI-exposed plants did not differ from that of control plants (Figure 3A). As expected, the acceptor-side limitation ($Y(NA)$) of the functional PSI centers in PSI-PI plants was substantially higher in all conditions compared to control plants (Figure 3A). PSI-PI treatment induced an approximately 50% decrease in PSII photochemistry ($Y(II)$) and corresponding increases in nonregulated energy dissipation ($Y(NO)$) and regulated energy dissipation ($Y(NPQ)$) in plants illuminated at light intensities of 50 and 100 $\mu\text{mol photons m}^{-2} \text{s}^{-1}$, whereas only minor differences in $Y(II)$, $Y(NO)$ and $Y(NPQ)$ were detected between PSI-PI-treated and control leaves at 0 and 500 $\mu\text{mol photons m}^{-2} \text{s}^{-1}$ (Figure 3B). These results indicated that the PSI-PI treatment impaired the light energy utilization of the PETC under light intensities, limiting photosynthesis. Importantly, however, changes in CO_2 concentration had very little effect on the quantum yields of PSI and PSII in both GL- and PSI-PI-treated plants.

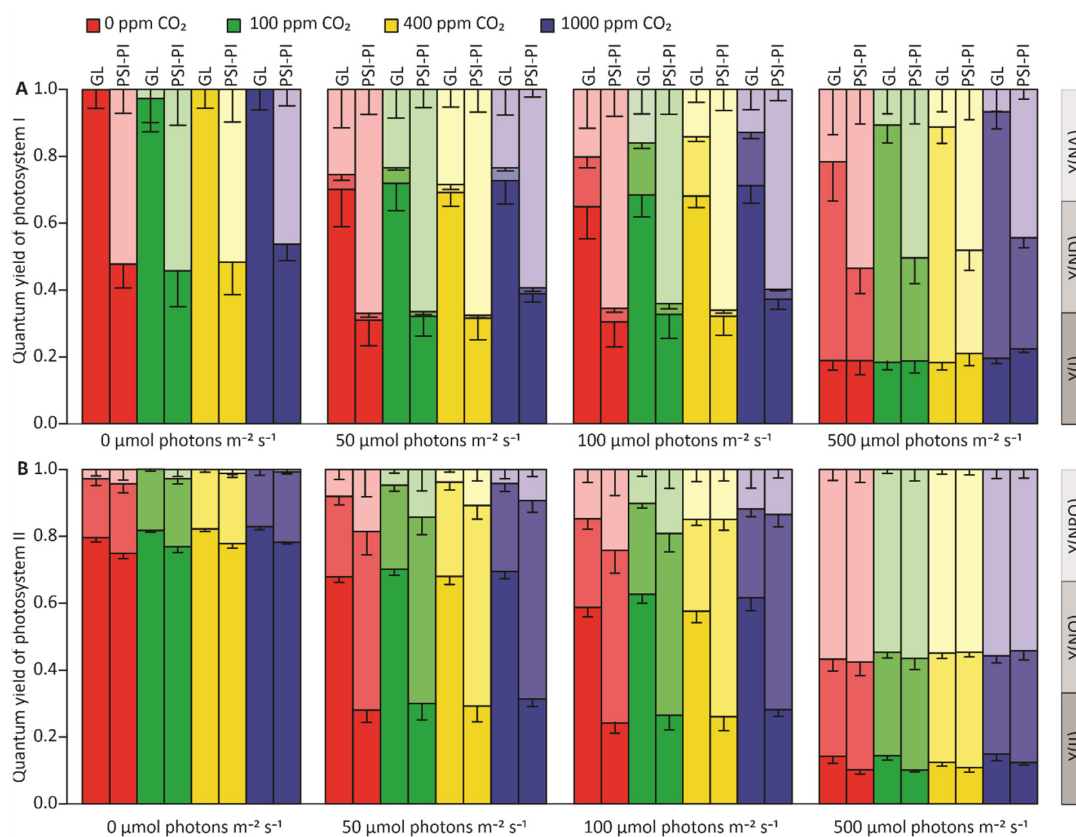


Figure 3. PSI and PSII quantum yields in *Arabidopsis* leaves illuminated under growth light (GL) or treated with PSI photoinhibition (PSI-PI) treatment at various CO_2 concentrations. GL plants were treated with growth light ($100 \mu\text{mol photons m}^{-2} \text{s}^{-1}$), and PSI-PI plants were treated with PSI photoinhibition light for three hours at CO_2 concentrations of 0 ppm, 100 ppm, 400 ppm, and 1000 ppm. After illumination, plants were dark-acclimated for 20 min and subsequently illuminated at 0, 25, 50, 100, and 500 $\mu\text{mol photons m}^{-2} \text{s}^{-1}$ for 3 min with Dual-PAM 100 for measurements of the quantum yield of functional photosystems. (A) PSI quantum yields: PSI photochemistry ($Y(I)$), PSI-donor-side limitation ($Y(ND)$), and PSI-acceptor-side limitation ($Y(NA)$). (B) PSII quantum yields: PSII photochemistry ($Y(II)$), nonregulated energy dissipation in PSII ($Y(NO)$), and regulated non-photochemical energy dissipation in PSII ($Y(NPQ)$). Error bars represent standard deviations ($p < 0.05$, $n = 8$).

3.2. Effects of Combined PSI-PI and Different CO₂ Treatments on Carbohydrate Accumulation and Stomatal Opening

To analyze the effect of PSI photoinhibition on the accumulation of photosynthetic carbon metabolites in leaves, we measured the starch, fructose, glucose, and sucrose contents, as well as the stomatal aperture, in GL- and PSI-PI-treated leaves.

Compared to GL plants, PSI-PI treatment did not significantly reduce the accumulation of glucose or fructose in leaves exposed to atmospheric or lower CO₂ concentrations, whereas PSI-PI-treated leaves had significantly higher amounts of these sugars at a high CO₂ of 1000 ppm (Figure 4A,B). The amount of sucrose was slightly, but not significantly, lower in PSI-PI-treated leaves compared to GL plants (Figure 4C). PSI-PI treatment had no effect on starch accumulation in leaves exposed to 0 or 100 ppm CO₂, whereas about 40 to 50% reduction in starch content was observed in PSI-PI-treated plants at 400 and 1000 ppm CO₂ (Figure 4D).

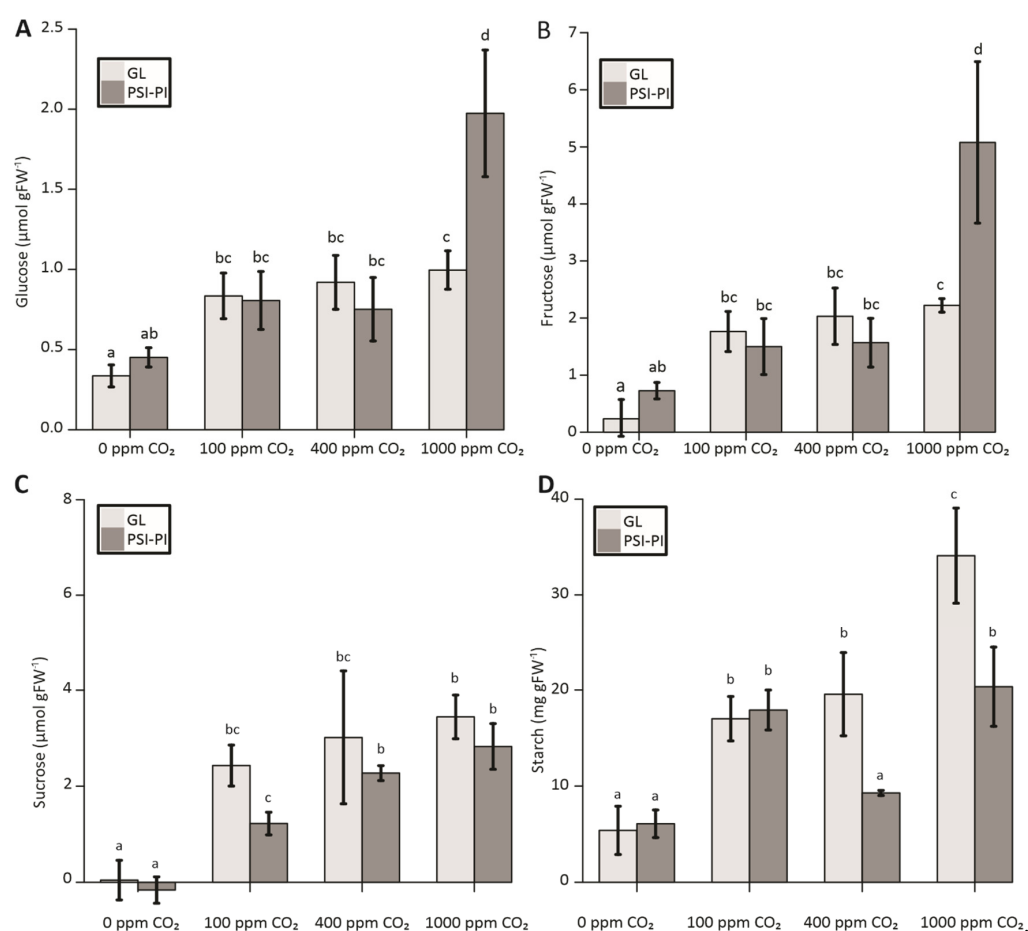


Figure 4. Starch and sugar contents in *Arabidopsis* leaves treated with either growth light of 100 μmol photons m⁻² s⁻¹ (GL; light gray) or with PSI photoinhibition (PSI-PI; dark gray) treatment for three hours at CO₂ concentrations of 0 ppm, 100 ppm, 400 ppm, and 1000 ppm. The quantification of starch and sugars was carried out with Megazyme assay kits and expressed as μmol per g fresh weight (FW) for glucose (A), fructose (B), and sucrose (C) and as mg per g FW for starch (D). SE, error bars (n = 5). Bars with different letters indicate significant differences with a *p*-value < 0.05 (ANOVA, Tukey HSD).

As it has been reported that leaf stomatal closure responds to CO₂ concentrations [36], we made leaf imprints and calculated the stomatal aperture index (width/length), which is indicative of stomatal conductance, after GL or PSI-PI exposure to various CO₂ concentrations (Figure S1). The stomatal aperture index was slightly but significantly higher in PSI-PI leaves in the absence of CO₂. At 1000 ppm CO₂, the stomatal aperture was significantly lower in both the control and PSI-PI-treated leaves compared to all other conditions.

3.3. Differential Gene Expression Induced by Exposure of Plants to PSI-PI Treatment and Different CO₂ Concentrations

3.3.1. Changes in Gene Expression Induced by Varying CO₂ Concentrations

First, we focused on differentially expressed genes (DEGs) in leaves exposed to CO₂ reduction and elevation relative to atmospheric CO₂ (Figure 5A–D). Abnormal CO₂ concentrations caused major changes in gene expression relative to 400 ppm CO₂, with only 10% overlap between the CO₂ treatments in GL-treated plants (Figure 5A,B) and 7% overlapping genes between the CO₂ treatments in PSI-PI-treated plants (Figure 5C,D). A minority (21% at 0 and 100 ppm; 7% at 1000 ppm) of the genes were differentially expressed in both the GL- and PSI-PI-treated plants (Figure S2).

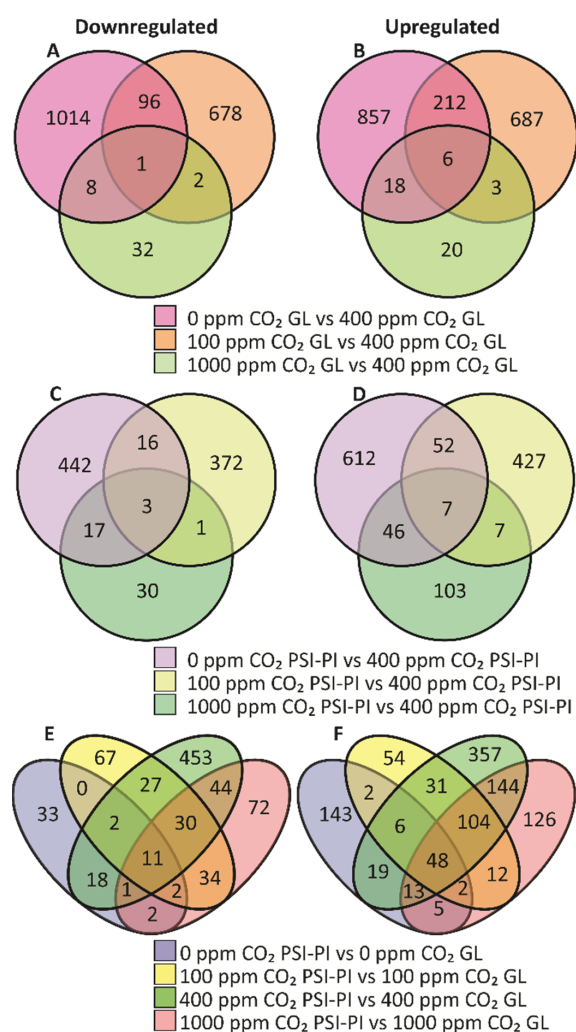


Figure 5. Venn diagrams of differentially expressed genes in plants treated either with growth light (GL) or with PSI photoinhibition (PSI-PI) at CO₂ concentrations of 0 ppm, 100 ppm, 400 ppm, and 1000 ppm. Downregulation (A) and upregulation (B) of genes in leaves exposed to different CO₂ concentrations at GL in comparison to plants exposed to 400 ppm (control) CO₂. Downregulation (C) and upregulation (D) of genes in leaves exposed to PSI-PI treatment at different CO₂ concentrations in comparison to plants exposed to PSI-PI treatment at 400 ppm CO₂. Downregulation (E) and upregulation (F) of genes in leaves exposed to PSI-PI treatment at different CO₂ concentrations in comparison to plants without PSI-PI treatment but at the same CO₂ concentration. The genes with $-1 \geq \log_2 \geq 1$ expression fold change with respect to relative controls and with a p -value < 0.05 are included in the figure. The list of the genes is presented in the Table S1.

The deprivation of CO₂ from the air induced a large number of DEGs with high fold-changes ($\log_2 > 4$) (Table S1). Interestingly, many of these genes were upregulated

in both GL- and PSI-PI-treated leaves (Table S1), indicating that the response was specifically related to CO₂ removal. Furthermore, the most highly induced genes included many involved in the biosynthesis of secondary metabolites (flavonoids, anthocyanins) derived from phenylalanine (Table 1). In total, we found 20 upregulated genes involved in flavonoid metabolism in GL- and PSI-PI-treated leaves exposed to 0 ppm CO₂. The genes encoding CHALCONE SYNTHASE (CHS) and DIHYDROFLAVONOL 4-REDUCTASE (DFR), key enzymes in flavonoid synthesis [37–39], were strongly induced at 0 ppm CO₂. CHS catalyzes the synthesis of naringenin chalcone, which is converted to naringenin by CHALCONE ISOMERASE (CHI). Naringenin is a precursor to several classes of flavonoids. DFR converts dihydroflavonols to flavan-3-ols, which serve as precursors for the synthesis of anthocyanins. The expression of the other genes encoding enzymes involved in flavonoid biosynthesis (UF3GT, AT5MAT, LDOX) or metabolism (GSTF12) was also upregulated at 0 ppm CO₂. Accordingly, CO₂ deprivation induced eight genes encoding MYB transcription factors (Table 1), which have previously been shown to regulate the biosynthesis of flavonoids [37,39,40]. Moreover, the bHLH, WRKY, and NAC transcription factors (TT8, GL3, TTG2, NAM, NAC032) (Table 1) are also involved in the regulation of the expression of flavonoid biosynthesis genes [37,39].

Low CO₂ (100 ppm) also significantly altered the gene expression, with 1685 DEGs in GL-treated plants and 885 DEGs in PSI-PI-treated plants compared to atmospheric CO₂ (Figure 5A–D). In contrast to the response to 0 ppm CO₂, the number of overlapping DEGs between GL and PSI-PE treatments was minimal (Table S1). Elevated (1000 ppm) CO₂ only slightly altered the gene expression in GL plants compared to atmospheric CO₂. The fold change in DEGs was also lower than in leaves exposed to 0 and 100 ppm CO₂ (Table S1).

All combinations of CO₂ and PSI-PI treatments resulted in a very low number of overlapping DEGs. Interestingly, however, the small number of DEGs upregulated in both GL- and PSI-PI-treated leaves at all divergent CO₂ concentrations included three genes encoding cytosolic and chloroplast COPPER/ZINC SUPEROXIDE DISMUTASE and a COPPER CHAPERONE for copper–zinc superoxide dismutase (Table S1). This suggested that superoxide scavenging may be an important function under the stress induced by changes in CO₂ concentration.

3.3.2. PSI-PI Treatment Induced Differential Expression of Unique Genes Involved in Iron Homeostasis and Light Receptor Signaling

Next, we analyzed changes in gene expression induced by PSI photoinhibition by identifying the DEGs in PSI-PI-treated leaves compared to GL-treated leaves at identical CO₂ concentrations (Figure 5E,F). As with the variation in the CO₂ concentration, the change in gene expression was mainly unique for each CO₂ level, with only 30% of the total DEGs overlapping. Interestingly, the highest number of PSI-PI-induced DEGs was observed in leaves treated with 400 ppm CO₂. Furthermore, the highest number of overlapping DEGs (10%) was found in leaves treated with 400 ppm and 1000 ppm CO₂, indicating that elevated CO₂ less drastically modified leaf metabolism than CO₂ deprivation, as is also evident in Figure 5A,B.

Fifty-nine genes differentially expressed in PSI-PI-treated plants at all CO₂ concentrations tested contained a high proportion of genes involved in iron (Fe) homeostasis (Table 2). Taking all CO₂ treatments together, twenty-two genes encoding proteins involved in Fe metabolism were differentially expressed in PSI-PI-treated leaves (Table 2). Genes encoding leaf-type and chloroplast-localized FERRITIN proteins (FER1, 3, and 4) were significantly upregulated in PSI-PI-treated leaves (Table 2). FERs are iron storage proteins that are induced by a local or temporal excess of Fe content in plants [41,42]. In addition to the FERs, eleven other Fe metabolism genes were upregulated by PSI-PI treatment (Table 2), including NEET, FRO1, 6, and 7, and VTL1 and 2 genes, encoding membrane proteins that are involved in the transportation of Fe or FeS clusters between the cytosol and organelles [43,44]. The upregulated genes CYTOSOLIC HEME BINDING PROTEIN1, 2, and 3 (*cHBP*) encode tetrapyrrole-binding proteins [45], and the expression

of *ENH1* and *AT3G49160* genes has been shown to be downregulated in response to iron deficiency [46,47]. On the other hand, the PSI-PI treatment repressed eight genes previously shown to be induced by Fe deficiency in plants (Table 2). The prominent upregulation of *FER* and Fe transporter genes and the concomitant repression of Fe-deficiency-induced genes in PSI-PI-treated leaves suggest that PSI photoinhibition causes the release of iron from PSI.

The DEGs regulated by PSI-PI treatment also included genes encoding light-signaling components with upregulated (*HY5*, *HYH*, *COL2*, *ARF*, *AT5G18404*, *SIG5*) or repressed (*RPGE1*, 3, and 4; *PIL1* and 2; *SIB1*) expression (Table 3). *HY5* protein acts downstream from light receptors during photomorphogenesis of seedlings (for reviews, see, e.g., [48,49]). *HYH* is homologous to *HY5* [50]. *CONSTANS-LIKE 2* (*CON2*), *ATTENUATED FAR-RED RESPONSE* (*ARF*), and *AT5G18404* belong to the phytochrome (Phy) signaling network [51,52], and *SIGMA FACTOR 5* (*SIG5*) controls chloroplast gene expression [53]. Besides the upregulation of light-signaling components, PSI-PI treatment significantly reduced the expression of genes encoding suppressors of light signaling (Table 3).

3.3.3. PSI-PI Treatment Upregulates Genes Encoding the Components of Cyclic Electron Flow, CBB Cycle, and Photorespiration

The different leaf treatments presented here induced a high number of moderate DEGs (fold change $-2 < \log_2 < 2$) (Table S1). To obtain an overall view of changes in nuclear gene expression, we conducted an enrichment analysis of DEGs to reveal the cellular functions targeted by changes in the CO₂ concentration or by the PSI-PI treatment. Several pathways related to chloroplast metabolism emerged from the analysis: PETC, sugar metabolism, and ROS and JA signaling (Table S2). To investigate the specific effect of PSI-PI treatment on the expression of photosynthetic genes, we compared the gene expression in PSI-PI-treated leaves with the corresponding result in GL leaves at each CO₂ concentration (columns 7 to 10 in Figure 6A). PSI-PI treatment, independently of the CO₂ concentration, moderately upregulated the genes encoding the subunits of chloroplast NAD(P)H DEHYDROGENASE-LIKE (NDH) complex and PROTON GRADIENT REGULATION (PGR) proteins (Figure 6A). These two complexes mediate electron flow from FD to thylakoid plastoquinone (PQ) pool via two different CEF pathways [54–57]. Accordingly, the genes encoding the leaf-type FDs (FD1 and FD2), the major photosynthetic isoforms participating in thylakoid electron transfer reactions, were upregulated by PSI-PI treatment (Figure 6A). At the same time, the root-type FD3 did not significantly respond to either PSI-PI treatment or changes in the CO₂ concentration. The expression of the genes encoding subunits of other thylakoid photosynthetic complexes was either not significantly changed (PSII, Cytb₆f, and ATPase) or slightly (PSI, LHCI) or moderately (LHCII) downregulated in PSI-PI-treated leaves at 100, 400, and 1000 ppm CO₂, with the decrease being the most pronounced in PSI-PI-treated leaves at ambient CO₂ concentration. The results in Figure 6A suggest that the PSI-PI treatment generally activates a signaling cascade that induces the expression of *CEF* genes and downregulates the expression of *LHCB* genes while having minimal effects on the expression of other PETC genes.

Next, we investigated how the expression of nuclear genes involved in the CBB cycle, photorespiration, and sugar metabolism directly derived from the CBB cycle responded to the PSI-PI treatment at different CO₂ concentrations. PSI-PI treatment upregulated many key enzymes in the CBB cycle and photorespiration (columns 7 to 10 in Figures 6B and S3), independently of the CO₂ concentration. The CBB genes involved in the carboxylation/oxygenation of RuBP (Rubisco and Rubisco activase), in the production of triose phosphates (GAP), and in the regeneration reactions of RuBP (RPI, TKL1, and PRK) were upregulated by PSI-PI treatment. The gene encoding the second isoform of TRANSKETOLASE, TKL2, did not respond to PSI-PI treatment (Figure 6B). TKL2 has been reported to be mainly expressed in seeds and senescing leaves [58], suggesting that it is not an important enzyme for photosynthetic carbon fixation.

Table 1. Differential expression of genes involved in flavonoid synthesis in response to CO₂ deprivation. The log₂ fold changes are presented in the columns (left to right): columns 1–3, changes induced by CO₂ concentrations under constant growth light (GL); columns 4–6, changes induced by CO₂ concentrations in PSI-PI-treated plants. Fold-change value is bolded when a $p < 0.05$.

Gene ID	Gene Name	Description		Log ₂ Fold Change					
				0 ppm CO ₂ GL vs. 400 ppm CO ₂ GL	100 ppm CO ₂ GL vs. 400 ppm CO ₂ GL	1000 ppm CO ₂ GL vs. 400 ppm CO ₂ GL	0 ppm CO ₂ PSI-PI vs. 400 ppm CO ₂ PSI-PI	100 ppm CO ₂ PSI-PI vs. 400 ppm CO ₂ PSI-PI	1000 ppm CO ₂ PSI-PI vs. 400 ppm CO ₂ PSI-PI
AT5G42800	<i>DFR</i>	Dihydroflavonol 4-reductase	Endoplasmic reticulum	10.52	−0.72	5.72	8.55	0.06	−0.22
AT5G17220	<i>GSTF12</i>	Glutathione S-transferase phi 12	Cytosol	8.08	−0.38	4.49	6.8	−0.18	0.6
AT5G54060	<i>UF3GT</i>	UDP-glucose:flavonoid 3-o-glucosyltransferase	Chloroplast	7.97	−2.74	4.28	6.9	0.25	1.51
AT3G29590	<i>AT5MAT</i>	HXXXD-type acyl-transferase family protein	Chloroplast	7.71	−0.7	3.33	5.83	−0.93	1.32
AT4G22880	<i>LDOX</i>	Leucoanthocyanidin dioxygenase	Nucleus	7.03	−0.43	2.2	6.82	−0.2	0.64
AT5G13930	<i>CHS</i>	Chalcone and stilbene synthase family protein	cytosol	5.99	−0.33	1.89	4.54	0.58	1.16
AT5G05270	<i>CHIL</i>	Chalcone-flavanone isomerase family protein	Chloroplast	2.9	0.89	0.59	1.76	1.37	0.63
AT1G66390	<i>MYB90</i>	Myb domain protein 90	Nucleus	8.19	0.3	6.25	5.94	−3.14	−1.52
AT4G09820	<i>TT8</i>	Basic helix-loop-helix (bHLH) DNA-binding superfamily protein	Cytosol	6.11	−0.42	3.89	5.24	−0.39	1.47
AT5G41315	<i>GL3</i>	Basic helix-loop-helix (bHLH) DNA-binding superfamily protein	Nucleus	4.31	1.92	2.88	3.17	−0.13	1.67
AT1G66370	<i>MYB113</i>	Myb domain protein 113	Nucleus	4.23	−2.88	0.73	5.21	−1.68	−1.4
AT2G37260	<i>TTG2</i>	WRKY family transcription factor family protein	Nucleus	3.14	1.66	1.3	1.9	0.75	0
AT1G56650	<i>MYB75</i>	Production of anthocyanin pigment 1	Nucleus	3.09	−1.04	1.34	2.99	−1.21	0.75
AT1G66380	<i>MYB114</i>	Myb domain protein 114	Nucleus	3.01	−3.1	0.87	4.97	0.85	2.17
AT2G47190	<i>MYB2</i>	Myb domain protein 2	Nucleus	2.66	0.31	0.4	1.09	−0.38	0.48
AT5G56840	<i>AT5G56840</i>	Myb-like transcription factor family protein	Nucleus	2.2	0.18	1.1	1.1	0.41	0.55
AT3G06490	<i>MYB108</i>	Myb domain protein 108	Nucleus	1.94	−0.32	0.73	2.25	−0.09	0.42
AT1G52880	<i>NAM</i>	NAC (No Apical Meristem) domain transcriptional regulator superfamily protein	Nucleus	1.69	0.56	0.59	1.35	0.11	−0.1
AT1G77450	<i>NAC032</i>	NAC domain-containing protein 32	Nucleus	1.53	0.6	−0.03	1.89	0.12	0.22
AT2G16720	<i>MYB7</i>	Myb domain protein 7	Nucleus	1.34	−0.23	0.38	2.03	0.08	0.78

Table 2. Differential expression of iron metabolism genes in leaves exposed to PSI photoinhibition (PSI-PI) treatment. The fold-change columns show log2 fold changes induced by PSI-PI treatment versus growth light (GL) treatment at different CO₂ concentrations indicated in the table. Fold-change value is bolded when $p < 0.05$.

Gene ID	Gene Name	Description	Localization	Log2 Fold Change			
				0 ppm CO ₂ PSI-PI vs. 0 ppm CO ₂ GL	100 ppm CO ₂ PSI-PI vs. 100 ppm CO ₂ GL	400 ppm CO ₂ PSI-PI vs. 400 ppm CO ₂ GL	1000 ppm CO ₂ PSI-PI vs. 1000 ppm CO ₂ GL
AT3G56090	<i>FER3</i>	Ferritin 3	Chloroplast	2.69	1.93	2.34	3.05
AT5G01600	<i>FER1</i>	Ferretin 1	Chloroplast	2.21	1.67	2.51	4.69
AT5G51720	<i>NEET</i>	2Fe–2S cluster binding protein	Chloroplast	1.91	1.14	1.38	1.97
AT2G40300	<i>FER4</i>	Ferritin 4	Chloroplast	1.37	0.86	1.15	2.15
AT3G49160	<i>AT3G49160</i>	Expression of the gene is downregulated in the presence of paraquat, an inducer of photooxidative stress. Downregulated by Fe deficiency.	Chloroplast?	1.32	1.67	1.64	3.52
AT5G17170	<i>ENH1</i>	Enhancer of SOS3-1/rubredoxin family protein	Chloroplast?	1.27	1.02	1.36	1.55
AT1G17100	<i>cHBP1</i>	Cytosolic heme-binding protein 1	Cytoplasm?	1.04	1.39	1.81	1.76
AT1G01590	<i>FRO1</i>	Ferric reduction oxidase 1	Plasma membrane	1.02	0.83	2.31	1.1
AT1G76800	<i>VTL2</i>	Vacuolar iron transporter (VIT) family protein	Vacuolar membrane	0.76	1.09	0.87	1.61
AT5G49740	<i>FRO7</i>	Ferric reduction oxidase 7	Chloroplast envelope	0.66	1.13	1.83	1.97
AT5G49730	<i>FRO6</i>	Ferric reduction oxidase 6	Plasma membrane	0.64	0.66	1.88	1.46
AT1G78450	<i>cHBP3</i>	Cytosolic heme-binding protein 3	Cytoplasm?	0.63	0.77	1.56	0.89
AT1G21140	<i>VTL1</i>	Vacuolar iron transporter (VIT) family protein	Vacuolar membrane	0.59	1.07	0.57	1.49
AT2G37970	<i>cHBP2</i>	Cytosolic heme-binding protein 2	Cytoplasm?	0.25	0.78	1.07	1.35
AT2G28160	<i>bHLH029</i>	basic helix-loop-helix, FER-like regulator of iron uptake	Nucleus	−0.6	−0.86	−1.05	−0.96
AT5G04150	<i>BHLH101</i>	Basic helix-loop-helix (bHLH) DNA-binding superfamily protein, response to Fe deficiency	Nucleus	−2.01	−1.82	−0.67	−3.51
AT3G56360	<i>AT3G56360</i>	Hypothetical protein, response to Fe deficiency	Plastid?	−2.44	−1.99	−2.43	−3.03
AT2G30766	<i>FEP1</i>	FE-uptake-inducing peptide 1, response to Fe deficiency	Cytoplasm or nucleus	−3.28	−3.66	−4.49	−4.92
AT1G47395	<i>FEP2</i>	Fe-uptake-inducing peptide 2, response to Fe deficiency	Cytoplasm or nucleus?	−3.7	−1.57	−4.33	−4.82
AT1G13609	<i>DEFL</i>	Defensin-like (DEFL) family protein, response to Fe deficiency	?	−4.04	−3.1	−4.54	−8.96
AT2G14247	<i>IRP3</i>	Iron-responsive protein 3	Chloroplast	−4.45	−4.05	−6.09	−8.79
AT5G05250	<i>AT5G05250</i>	Hypothetical protein, response to Fe deficiency	?	−5.1	−5.9	−6.36	−6.31

Table 3. Differential expression of light-signaling genes in leaves exposed to PSI photoinhibition (PSI-PI) treatment. The fold-change columns show log₂ fold changes induced by PSI-PI treatment versus growth light (GL) treatment at different CO₂ concentrations indicated in the table. Fold-change value is bolded when $p < 0.05$.

Gene ID	Gene Name	Description	Localization	Log ₂ Fold Change			
				0 ppm CO ₂ PSI-PI vs. 0 ppm CO ₂ GL	100 ppm CO ₂ PSI-PI vs. 100 ppm CO ₂ GL	400 ppm CO ₂ PSI-PI vs. 400 ppm CO ₂ GL	1000 ppm CO ₂ PSI-PI vs. 1000 ppm CO ₂ GL
AT5G11260	<i>HY5</i>	Long hypocotyle 5, bZIP transcription factor	Nucleus	1.96	2.03	2.53	2.07
AT3G17609	<i>HYH</i>	HY5-homolog	Nucleus	1.69	2.06	2.27	2.55
AT3G02380	<i>COL2</i>	CONSTANS-like 2	Nucleus	1.49	1.65	2.23	1.71
AT2G24540	<i>AFR</i>	Attenuated far-red response	Cytoplasm?	1.36	1.9	2.29	2.09
AT5G18404	<i>AT5G18404</i>	Small protein, response to red or far-red light	Nucleus	1.36	1.06	1.66	1.14
AT5G24120	<i>SIG5</i>	Sigma factor 5, regulation of plastid genes	Chloroplast	1.02	2.04	2.46	1.89
AT3G62090	<i>PIF6/PIL2</i>	Phytochrome interacting factor 3-like 2	Nucleus	0.04	−1.39	−0.57	−1.54
AT1G10657	<i>RPGE4</i>	Repressor of photosynthetic genes 4	Nucleus	−0.06	−0.65	−1.29	−0.25
AT3G56710	<i>SIB1</i>	Sigma factor binding protein 1	Chloroplast	−0.16	−0.74	−1.47	−0.83
AT3G55240	<i>RPEG3</i>	Repressor of photosynthetic genes 3	Nucleus	−1.1	−2.28	−2.38	−1.94
AT5G02580	<i>RPGE1</i>	Repressor of photosynthetic genes 1	Nucleus	−2	−2.69	−2.39	−2.68
AT2G46970	<i>PIF2/PIL1</i>	Phytochrome-interacting factor 3-like 1	Nucleus	−2.28	−2.66	−2.5	−2.56

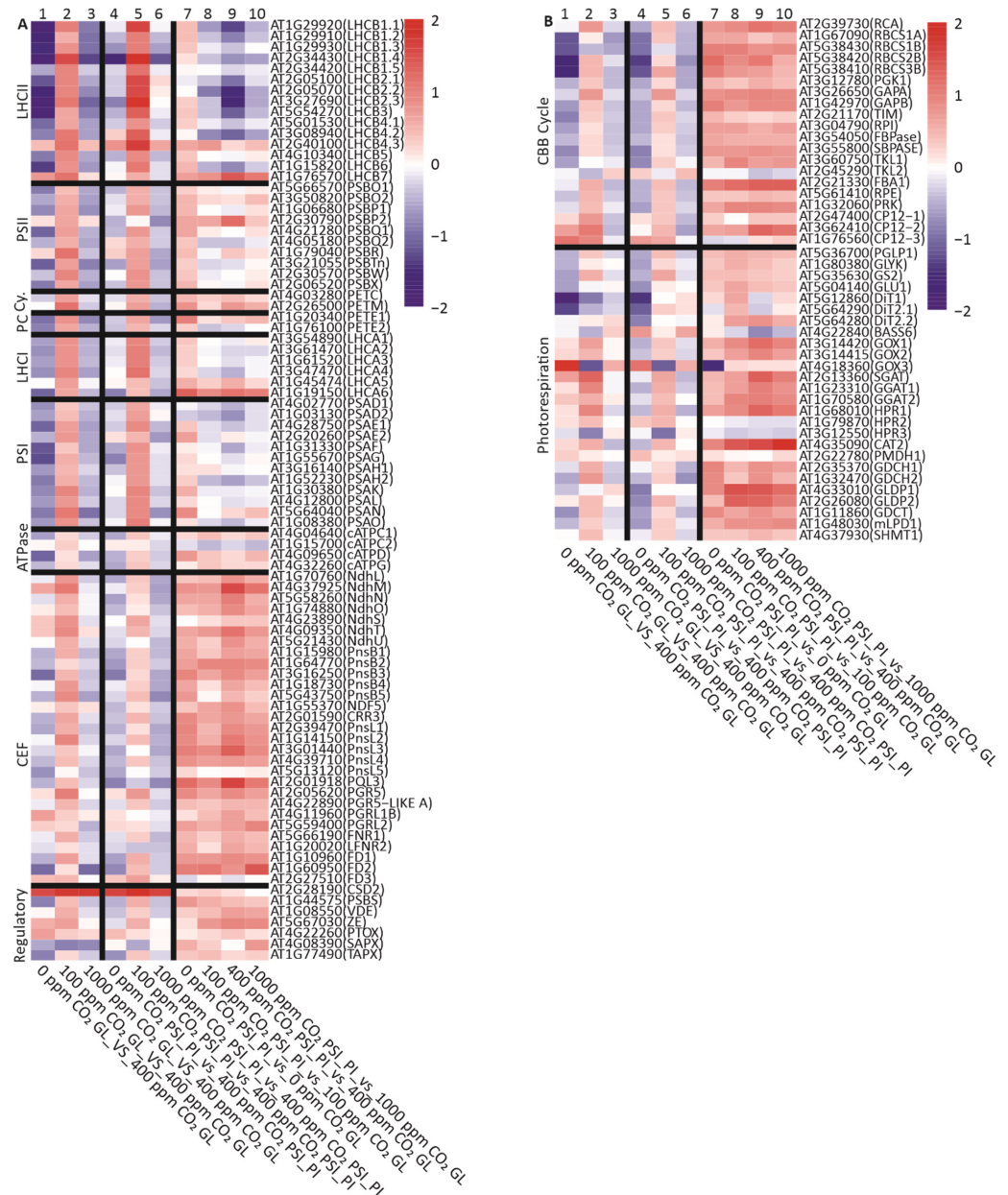


Figure 6. Differential expression of nuclear genes encoding proteins involved in (A) photosynthetic electron transport chain (PETC) and (B) Calvin–Benson–Basshan (CBB) cycle and photorespiration pathways. The heatmap shows the log₂ values of differentially expressed genes in plants exposed to growth light (GL) and specific PSI photoinhibition (PSI-PI) treatment for three hours at various CO₂ concentrations. The treatments compared in the columns are indicated under the figure. Columns: 1–3, changes induced by abnormal CO₂ concentrations under constant growth light; 4–6, changes induced by abnormal CO₂ concentrations in PSI-PI-treated plants; 7–10, changes induced by PSI-PI treatment at various CO₂ concentrations indicated in the figure. The gene lists were compiled manually to include all nuclear genes encoding PETC subunits as well as CBB cycle and photorespiratory enzymes (Table S3). Cy.: *Cytb₆*; PC: plastocyanin.

In the photorespiration pathway, several genes encoding peroxisomal enzymes showed higher expression in PSI-PI-treated leaves compared to GL leaves (Figures 6B and S3) [59]. The expression of the peroxisomal *CATALASE2* (*CAT2*) gene was significantly induced by PSI-PI treatment (Figure 6B). Furthermore, the expression of genes encoding enzymes that process the photorespiratory amino acid intermediates (*GGAT1*, *GGAT2*, and *SGAT*) was also upregulated in response to the PSI-PI treatment, as well as the *HPR1* gene encoding the

enzyme producing glycerate in the final phase of photorespiration (Figures 6B and S3). In addition to peroxisomal enzymes, the expression of genes encoding mitochondrial enzymes involved in photorespiration was also upregulated by the PSI-PI treatment, especially genes encoding enzymes that catalyze the production of serine from glycine (GLDP1, GLDP2) (Figures 6B and S3).

The genes involved in the synthesis and degradation of starch and sucrose did not show any clear differential expression patterns induced by either the PSI-PI treatment or changes in the CO₂ concentration (Figure S4). Although PSI-PI treatment reduced the accumulation of starch at atmospheric and elevated CO₂ concentrations (Figure 3), the expression of genes encoding chloroplast starch synthesis were not significantly differentially expressed in these leaves (Figure S4).

3.3.4. Search for the Origin of Regulatory Signals Generated by PSI-PI Treatment at Different CO₂ Concentrations

To identify the origin of the chloroplast-generated retrograde signals produced by the PSI-PI treatment and changes in the CO₂ concentration, we next collected the genes known from the literature to be induced by potential initiators of chloroplast signaling (¹O₂, H₂O₂, oxylipins, JA, HL, and nitric oxide (NO)) and analyzed their expression with our experimental setup (Figure 7 and Figures S5 and S6). The majority of genes known to respond to OPDA and JA were upregulated in GL- and PSI-PI-treated leaves exposed to 0 ppm CO₂ (columns 1 and 4 in Figure 7C,D), indicating that the major signals regulating the nuclear gene expression at 0 ppm are likely to be mediated by OPDA and/or JA. Only about 50% of the genes responding to ¹O₂ or H₂O₂ were induced in GL- and PSI-PI-treated leaves exposed to 0 ppm CO₂ (columns 1 and 4 in Figure 7A,B), suggesting that these are less likely to be the signaling molecules. The DEG profiles at 100 ppm CO₂, with respect to 400 ppm, suggested that neither ¹O₂ nor JA signaling (columns 2 and 5 in Figure 7A,D) explain the change in gene expression in leaves exposed to 100 ppm CO₂. The exposure of leaves to 1000 ppm CO₂ did not activate any of the systematic signals analyzed in Figure 7.

The PSI-PI treatment at 400 ppm CO₂ did not activate either JA- or ¹O₂-responsive genes (column 9 in Figure 7C,D), indicating that the origin of DEGs cannot be traced to these compounds. On the other hand, only 40% of OPDA-responsive genes were slightly activated by the treatment, and only 30% of H₂O₂-responsive genes were moderately upregulated (column 9 in Figure 7B,C), suggesting that the signal(s) induced by the PSI-PI treatment at atmospheric CO₂ may be only partially related to the signaling cascades induced by these compounds.

In addition to ROS, NO has also been reported to induce *FER* gene expression, followed by Fe accumulation in plant tissues [41]. Therefore, we tested whether the NO-responsive genes [60,61] would also respond to the PSI-PI treatment (Figure S5). In general, no similar gene expression profiles typical of NO treatment were observed in PSI-PI-treated leaves (columns 7 to 10 in Figure S5). Only *FER1* was significantly induced, suggesting that the changes in nuclear gene expression in PSI-PI-treated leaves were not caused by NO signaling.

The fluctuating-light regime included in our PSI-PI treatment comprised short pulses of high-intensity light (see Materials and Methods), which may trigger the signaling cascades observed in HL-exposed leaves. We therefore compared our transcriptomic data with those published by Alvarez-Fernandez [62], where *Arabidopsis* plants were transferred from 150 to 1100 μmol photons m⁻² s⁻¹ for 3.5 h. We took the genes that were most up- and downregulated by the PSI-PI treatment (Table S1) and analyzed how the expression of these genes had changed after the 3.5 h HL treatment reported by Alvarez-Fernandez [63]. Approximately 70% of the genes most upregulated by PSI-PI treatment were also induced by HL, whereas most of the genes downregulated by PSI-PI did not respond to the HL treatment (Figure S6). The comparison of Fe homeostasis DEGs after the PSI-PI treatment with the HL treatment indicated that *FERs*, *CHBP1*, and *ENH1* were induced by HL, while most of the Fe-deficiency genes suppressed by PSI photoinhibition (Table 2) did not respond

to the HL treatment (Figure S6). This indicated that although the transcript profiles after PSI-PI treatment and HL had some similarities, 50% inhibition of PSI also had a specific and partially stronger effect on nuclear gene expression than HL alone.

To gain further insight into the signaling cascade induced by the PSI-PI treatment at different CO₂ concentrations, we used the Genevestigator database [63] and searched for experiments where light conditions were modified or the plants were treated with ROS, OPDA, JA, or elevated CO₂, and then we analyzed the expression of PETC, CBB, and photorespiratory genes in these accessions (Figure S7). Only the extreme light change experiment, in which mature plants grown at very low light intensity were transferred to 100-times higher light intensity for 6 h, gave a similar pattern of photosynthetic gene expression to that observed in plants after the PSI-PI treatment (Figure 6): the upregulation of CEF, CBB, and photorespiratory genes and the downregulation of LHCB genes. Thus, the redox imbalance induced by PSI-PI treatment in the chloroplast resembles the conditions created by a strong increase in light intensity in the plant environment.

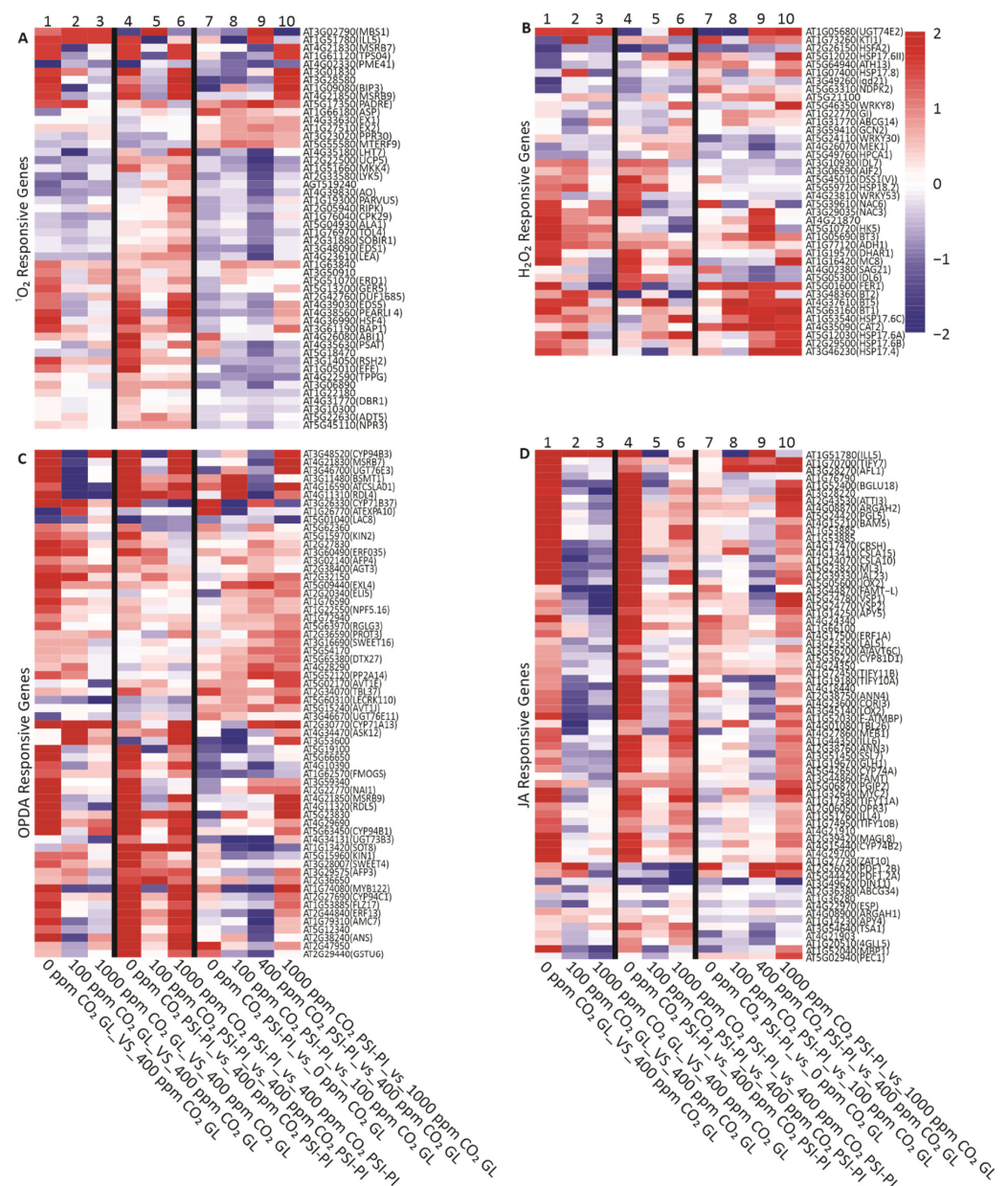


Figure 7. Differential expression of genes induced by various signaling molecules in *Arabidopsis thaliana* leaves exposed to GL and PSI photoinhibition (PSI-PI) treatment at CO₂ concentrations of

0, 100, 400, and 1000 ppm. The heatmap shows the log₂ values of the genes upregulated by (A) singlet oxygen (¹O₂), (B) hydrogen peroxide (H₂O₂), (C) 12-oxo-phytodienoic acid (OPDA), and (D) jasmonic acid (JA). The genes used in the analyses are listed in Table S3. The plant treatments are indicated below each column. The ¹O₂ gene list consists of genes reported to be ¹O₂-responsive in Op Den Camp et al. [64], with the addition of genes included in the following GO terms: singlet-oxygen-mediated programmed cell death (GO:0010343), response to singlet oxygen (GO:0000304), cellular response to singlet oxygen (GO:0071452). The H₂O₂ gene list consists of genes included in the following GO terms: response to oxidative stress (GO:0006979), hydrogen peroxide catabolic process (GO:0042744), cellular response to hydrogen peroxide (GO:0070301). The OPDA and JA gene list consists of genes reported to be OPDA- or JA-responsive in Gollan and Aro [22]. The columns are described in Figure 6.

4. Discussion

4.1. PSI-PI Treatment of Leaves Induces Similar PSI Photoinhibition Independent of CO₂ Concentration

In this study, we focused on the influence of PSI-acceptor-side components on the susceptibility of PSI to light damage and on the global transcriptomic changes induced by the imbalanced function of the PETC. To this end, *Arabidopsis* plants were exposed to various CO₂ concentrations simultaneously with an artificial fluctuating-light (PSI-PI) treatment that specifically induces PSI damage with only minor effects on PSII function (Figure 2) [25]. It has been shown that PSI photoinhibition in *Arabidopsis* is caused by damage to FeS clusters in PSI [12]. Previously, we reported that PSI-PI treatment significantly decreases the CO₂ assimilation rate [28,65]. However, as shown in Figure 2C, a similar decrease in PSI occurred independently of the CO₂ concentration, indicating that neither the reduction nor the elevation in the CO₂ level significantly affected the susceptibility of PSI to photoinhibition. This finding may indicate that there is no substantial influence of CO₂ on the oxidation state of PSI in our experimental setup. It is therefore conceivable that over-reduction by PSI during the PSI-PI treatment destroys FeS clusters more rapidly than oxidized FD can accept electrons from PSI. It is also likely that the artificial PSI-PI treatment does not directly mimic any natural stress conditions inducing PSI photoinhibition, although the damage to PSI FeS clusters seems to also occur similarly during cold-induced PSI photoinhibition [66]. Nevertheless, the PSI-PI treatment is a useful tool to investigate the stress symptoms initiated by changes in the internal CO₂ concentration of leaves and occurring concomitantly with damage to PSI. For example, a fluctuating natural light environment combined with drought may damage the function of PSI but simultaneously induce stomatal closure, thereby decreasing the internal CO₂ concentration in leaves. Likewise, sudden cold weather during the springtime causes a decline in stromal enzyme activities but is often combined with bright daylight, causing over-reduction by the PETC and damage to PSI.

PSI-PI treatment at 400 and 1000 ppm CO₂ had the strongest effect on leaf carbon metabolism (Figure 4). The accumulation of starch was reduced by half, whereas the content of monosaccharides (glucose and fructose) was nearly doubled at high CO₂ (Figure 4). Yet, no differences in stomatal aperture were detected between GL- and PSI-PI-treated leaves at 400 or 1000 ppm CO₂ (Figure S1), indicating that the lower starch content of PSI-PI-treated leaves is not due to stomatal function. Chloroplast starch synthesis is regulated by ADP-glucose pyrophosphorylase (AGPase), a redox-regulated enzyme activated under light by thioredoxins [67,68]. PSI-PI treatment, however, causes the oxidation of stromal enzymes [28], suggesting that the reduced starch synthesis in PSI-PI-treated leaves results from AGPase inactivation, with a consequent imbalance in leaf carbon metabolism. This conclusion is supported by the observation that impaired starch synthesis in chloroplasts increases the accumulation of glucose and fructose in leaves [69]. Imbalanced starch metabolism may impair plant growth for days after the termination of PSI-PI stress because, firstly, the repair of photodamaged PSI centers is a very slow process [6,7,65], and

secondly, the chloroplast starch reservoirs are an important energy source for diel plant growth [70–72].

4.2. CO₂-Specific Changes in Gene Expression: Removal of CO₂ Activates Flavonoid Metabolism, Likely via JA/OPDA Signaling in Leaves

Genes that strongly responded to 0 ppm CO₂ are shown to encode enzymes and transcription factors involved in metabolic pathways for the production of flavonoids (Table 1). Flavonoids are antioxidants that play a critical role in plant interactions with their environments [73], and recently, Banerjee et al. [74] demonstrated that the levels of flavonoids increase in the absence of CO₂. Here, we found that 20 genes involved in flavonoid biosynthesis were upregulated in response to CO₂ deprivation, including 7 biosynthetic enzymes and 13 transcription factors (Table 1). The upregulation of these MYB genes is likely to lead to the activation of flavonoid biosynthesis genes [37,39,75,76]. R2R3-MYB transcription factors (MYB75, MYB90, MYB113, and MYB114) form an R2R3-MYB/bHLH/WD40 complex with GL3/EGL3/TT8 and TTG1 transcription factors [77,78]. This complex specifically activates the expression of enzymes that catalyze flavonoid synthesis and anthocyanin metabolism [37,78].

JA mediates the accumulation of flavonoids by inducing the expression of R2R3-MYB genes and flavonoid synthesis genes [16,23,79,80]. It has been shown that JA receptor mutants exhibit a deficiency in the expression of MYB and flavonoid synthesis genes [23]. Our findings indicate that genes responsive to JA and OPDA are upregulated when CO₂ is removed from the environment (Figure 7C,D). The upregulation of JA-responsive genes could be triggered by an increase in the production of ROS due to the over-reduction of the PETC, which leads to the synthesis of JA [81,82]. JA then induces the expression of genes by activating the R2R3-MYB/bHLH/WD40 complex, which induces the expression of flavonoid synthesis genes. Flavonoids, being effective scavengers of ROS, can then protect the plant from oxidative stress.

4.3. PSI Photoinhibition Changes the Expression of Nuclear Genes Involved in Iron Homeostasis, Light Signaling, and PSI-Acceptor-Side Metabolism

PSI-PI treatment induced the differential expression of 59 genes independently of the CO₂ concentration (Table S1) and 200 genes in three out of the four differential CO₂ treatments applied in this study (Figure 5). Interestingly, the leaves exposed to the PSI-PI treatment at atmospheric CO₂ revealed the highest number of DEGs (810 genes in total) (Figure 5), indicating that, in total, over 1000 genes responded specifically to the PSI-PI treatment.

PSI-PI treatment induced 24 genes involved in plant Fe homeostasis (Table 2), which is consistent with damage to FeS clusters during PSI photoinhibition [12,66]. Although the PSI-PI treatment does not lead to the degradation of PSI subunits during illumination [28], the damage to FeS clusters may induce the release of Fe from PSI complexes, leading to excess-Fe stress in the chloroplast. Twelve genes induced by PSI photoinhibition are involved in Fe uptake into the cell and cell organelles (FROs, VTLs), Fe cofactor transport (NEET, cHBPs), and Fe storage (FERs) (recent review by Sági-Kazár et al. [44]). FERRIC REDUCTION OXIDASE (FRO) proteins are membrane proteins that catalyze the reduction of Fe⁺³ to Fe⁺² and thereby facilitate the Fe uptake across the plasma and organelle membranes [43,83]. FRO7 is a part of an iron translocator that transports Fe to the chloroplast [83], and VACUOLAR IRON TRANSPORTERS (VTR) are involved in Fe transport to the vacuole [44]. The majority of Fe in leaves is incorporated into heme and FeS clusters in organelles. FeS clusters are also required in the cytosol, and both chloroplastic and mitochondrial NEET proteins have been proposed to deliver 2Fe-2S clusters from organelles to cytosolic proteins [84]. The cHBPs carry hemes in the cytoplasm, although their physiological role is still unknown. FER genes are induced by Fe excess in plants but also by other stresses, including HL stress (Figure S6) [41,62,85]. Accordingly, the genes involved in the induction and the co-expression network of Fe deficiency were highly repressed in PSI-PI-treated leaves (Table 2) [86–88].

FERs bind iron and sequester it in an inert form, thereby protecting cells from oxidative damage by the Fenton reaction [44]. Indeed, the degradation of PSI complexes in *Chlamydomonas* has been shown to induce the accumulation of FER proteins [89], suggesting that an increased risk of Fe release from PSI proteins activates *FER* gene expression. Consistently, in the *pgr5* mutant, which suffers from severe PSI photoinhibition under HL [90], *FERs* and iron transporter genes are induced by HL illumination [91]. We postulate that the damage to PSI induces the release of Fe from PSI FeS clusters in the chloroplast and that such an excess of Fe in turn initiates a signal from the chloroplast to the nucleus (Figure 8). This signal upregulates the expression of genes involved in Fe homeostasis, whereas the genes known to be induced by Fe deficiency in plants, are simultaneously repressed by PSI photoinhibition (Table 2; Figure 8).

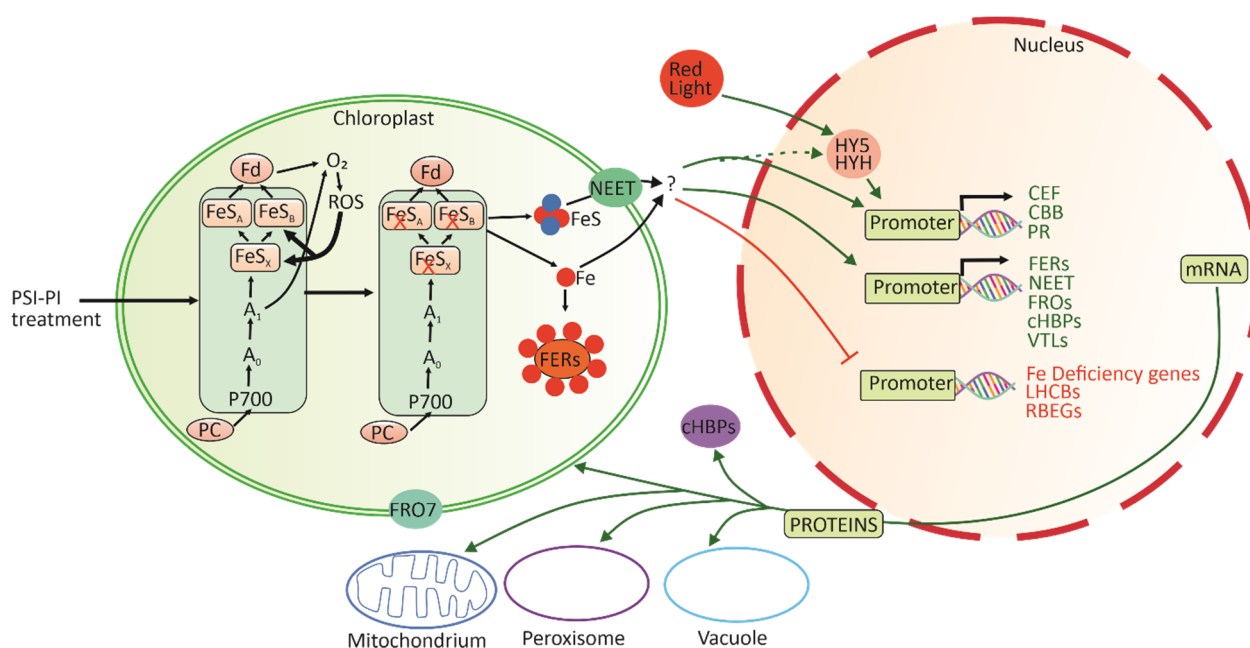


Figure 8. Scheme for the chloroplast retrograde signaling pathway controlling nuclear gene expression in PSI-photoinhibited leaves. PSI-PI treatment induces the accumulation of electrons on the acceptor side of PSI, which increases ROS production, followed by damage to FeS centers in PSI (FeS_A , FeS_B , FeS_X). Damage to FeS centers may lead to the release of iron. Iron is scavenged by ferritins (FERs), but when the iron content exceeds the binding capacity of FERs, the rise in iron concentration initiates a retrograde signaling cascade, activating iron homeostasis genes responding to excess iron and repressing iron-deficiency genes. The signal also activates the genes encoding PSI-acceptor-side pathways, cyclic electron flow (CEF), the Calvin–Benson–Bassham (CBB) cycle, and photorespiration (PR). Alternatively, FeS centers may be released from the damaged PSI and transported to the cytosol via NEET protein, transferring the signal from the chloroplast to the nucleus. The mediators of the signaling cascade are unknown. Furthermore, the expression of CEF, CBB cycle, and PR genes may also be regulated by a combination of red-light-induced transcription factors like HY5 and HYH and Fe signaling.

PSI-PI treatment also targeted a group of light-signaling regulators by inducing or repressing the expression of the respective genes (Table 3). The *HY5*, *HYH*, *COL2*, and *ARF* genes encode nuclear-located transcription factors that activate light-responsive genes. The influence of the master transcription factor HY5 on the activation of light-regulated genes during photomorphogenesis is well established (for reviews, see, e.g., [48,49]), while much less is known about the function of HY5 and HYH in later stages of leaf development and in mature leaves. HY5 has been reported to be expressed in various organs of adult tomato plants, including roots [92], and its expression has been shown to increase in response to high [93] and UV-B light [94]. HY5 is also linked to several hormone- and

stress-signaling cascades [16,48,49,95], and it has been suggested to act downstream of chloroplast retrograde signaling to the nucleus [16,96,97]. Our transcriptomic data indicate that HY5 and HYH expression can also be induced by exposing mature leaves to fluctuating light, which causes PSI photoinhibition (Table 3). Chloroplast-localized SIG5 is a member of the plant sigma factor family, and this gene is induced by several stresses [98]. It controls the activity of plastid-encoded RNA polymerase (PEP), which is responsible for the transcription of plastid photosynthetic genes [99]. The upregulation of SIG5 in PSI-photoinhibited leaves suggests that stress not only affects nuclear gene expression but also affects plastid gene expression via the regulation of PEP polymerase.

In addition to the induction of light-signaling transcription factors, PSI-PI treatment significantly reduced the expression of genes encoding suppressors of photomorphogenesis (PIF2/PIL1, PIF6/PIL2) and photosynthetic gene expression (RPGEs) (Table 3). GOLDEN2-LIKE transcription factors (GLKs) are potential targets of RPGE regulation. GLKs function as dimers, and they primarily activate nuclear genes encoding photosynthesis proteins by binding to the CCAATC sequence in the promoter region [100]. RPGEs inhibit the binding of GLKs to DNA by specifically interacting with GLK proteins and disrupting GLK dimerization [101]. In our experiment, GLK genes were not differentially expressed, but the significant repression of RPGE genes in PSI-PI-treated leaves compared to GL-treated leaves may release GLK proteins from the inhibitory RPGE complex and allow the post-translational activation of GLKs by dimerization.

PSI-PI treatment modifies photosynthetic metabolism in chloroplasts, and, accordingly, genes encoding chloroplast proteins were highly represented among the DEGs in PSI-PI-treated leaves (Table S1). A special focus on the differential expression of photosynthetic genes revealed that PSI photoinhibition increased the expression of genes encoding electron acceptors of PSI: CEF, CBB cycle, and photorespiration components (Figure 6). In the future, this finding needs to be confirmed by proteomic analyses. Of the enzymes comprising both photosynthetic and non-photosynthetic isoforms, only the photosynthetic isoforms showed differential expression in PSI-PI-treated leaves compared to GL leaves, emphasizing the specificity of the signal. A photosynthetic DEG profile similar to that induced by the PSI-PI treatment was found only in the leaves exposed to HL at 100 times the intensity of growth light (Figure S7), the light intensity most likely to induce strong PSI photoinhibition in leaves.

4.4. Origin of the Signal(s) Initiating PSI Photoinhibition-Responsive Expression of Nuclear Genes

Three potential sources of the signal(s) initiating the differential expression of nuclear genes during the PSI-PI treatment of leaves can be envisaged. Such predictions, based on the light quality of the PSI-PI treatment, changes in chloroplast redox states during the treatment, and the DEG profiles obtained from treated leaves, include the following options as sources and putative signaling pathways: (i) low-intensity red-light pulses of fluctuating light inducing Phy signaling, (ii) redox imbalance in PETC components and the consequent generation of ROS signaling, and (iii) excess Fe stress in chloroplasts inducing putative retrograde signaling.

Option (i) Theoretically, the short low-intensity red-light pulses in the fluctuating-light regime could directly promote Phy-mediated regulation of nuclear gene expression, which could explain the higher expression of HY5/HYH transcription factors and the other positive effectors and the concomitant downregulation of specific light signaling repressors in PSI-PI-treated leaves (Table 3). Nevertheless, Phy generally activates the expression of photosynthetic genes under light (Figure S7, dark to light) [17], whereas we observed the selective induction and repression of photosynthetic genes by the PSI-PI treatment (Figure 6). Accordingly, the red-light pulse of the PSI-PI treatment may be responsible for the differential expression of Phy-related transcription factors and repressors but cannot fully explain the expression profiles of photosynthetic genes in PSI-PI-treated leaves. Alternatively, PSI photoinhibition may initiate chloroplast retrograde signal(s) that alter the expression/function of nuclear light-responsive transcription factors and

repressors (Figure 8), as recently demonstrated under stresses caused by the dysfunction of chloroplast biogenesis (see recent reviews [15–17]).

Option (ii) PSI-PI treatment over-reduces the redox components between PSI and PSII [28], leading to a redox imbalance between the light and carbon fixation reactions in chloroplasts, which in turn can increase ROS production in thylakoid complexes [90]. Both the redox imbalance and ROS generation have been shown to initiate redox signals from the chloroplast to control the nuclear gene expression. Since the redox imbalance induced by PSI-PI treatment mimics that induced by the HL treatment, we compared the DEGs induced in PSI-PI-treated leaves with recently published transcriptomic data on the induction of photosynthetic genes upon the HL treatment of plants (Figure S6) [62,102]. This analysis revealed that the strongest DEGs present in PSI-PI-treated leaves (Tables 2 and 3) were expressed in leaves exposed to HL for 3.5 h (Figure S6) [62]. Approximately 70% of the genes upregulated by our PSI-PI treatment were also upregulated by HL, whereas most of the genes downregulated by PSI-PI did not respond to the HL treatment (Figure S6). However, most of the genes encoding CEF, CBB cycle, and photorespiration components were not differentially expressed in response to HL [62,102], contrary to their DEG behavior in the PSI-PI treatment. This suggests that the stress induced by PSI-PI treatment is, at least in part, different from that induced by HL and likely relays additional signals from chloroplasts to the nucleus.

Singlet oxygen and H_2O_2 are the major stress-induced ROS produced by photosynthetic light reactions. In mature leaves, photodamaged PSII is a major source of 1O_2 in the chloroplast, while PSI donates electrons to molecular oxygen, leading to the generation of superoxide and H_2O_2 [103]. This prompted us to test whether the genes known to be induced by 1O_2 and H_2O_2 were upregulated in our experimental setup (Figure 7). Very few of the genes known to be induced by 1O_2 were upregulated upon PSI-PI treatment (Figure 7), consistent with a very weak inhibition of PSII in treated leaves (Figure 2). H_2O_2 does not seem to act as a major signal modifying nuclear gene expression, as only two genes (*CAT2* and *FER1*) are strongly upregulated in PSI-PI-treated leaves (Figure 7). It is likely that, despite the imbalanced redox state in the chloroplast, there is no increased production of ROS in leaves with prolonged PSI photoinhibition [90], probably due to the enhanced non-photochemical quenching of energy in damaged PSI [12,28]. Furthermore, the known JA/OPDA-induced genes, whose products have been suggested to mediate thylakoid-initiated retrograde signaling [22,23], were mostly downregulated or did not respond at all to the PSI-PI treatment (Figure 7).

Option (iii) Only one PSI-PI-treatment-specific trigger for retrograde signaling from chloroplasts to the nucleus was possible to be traced based on our experiments and data analyses. PSI-PI treatment induced severe PSI inhibition, which is initiated by damage to the FeS clusters [12,66]. We propose that the release of Fe from the photodamaged PSI complex causes excess-Fe stress in the chloroplast, which initiates a retrograde signal to the nucleus (Figure 8). This chloroplast signal targets the genes that alleviate Fe stress, facilitate Fe transport, and improve the acceptor-side sink capacity of PSI. The production of hydroxyl radicals via the Fenton reaction between H_2O_2 and Fe^{+2} [10] may originally initiate the cascade, although OPDA signaling, generally associated with lipid peroxidation by hydroxyl radicals [104], was not particularly activated by the PSI-PI treatment (Figure 7C). Alternatively, FeS centers may be released from the damaged PSI and transported to the cytosol via the NEET protein (Figure 8). Such an effect on nuclear gene expression partially mimics the HL stress, while the effect is stronger and more selective than that observed when only increasing the light intensity (Figure S6). It has been reported that HL alone, without any fluctuating-light treatment, damages the PSI FeS_A and FeS_B clusters, while under strong PSI photoinhibition, the FeS_X cluster is also damaged [12], suggesting that strong PSI photoinhibition induces more severe excess-Fe stress than a moderate increase in light intensity. PSI-PI-treatment- and HL-induced stress distinctively differ from each other by the fact that HL stress also induces the strong photoinhibition of PSII, together with ROS production [105,106], which is not observed in the PSI-PI treatment [90]. A literature

search of DEG profiles shows that both PSI-PI and HL treatments induce genes generally associated with excess-Fe stress (Table 2, Figure S7), whereas the well-defined ROS signaling resulting from HL is absent in PSI-PI-treated leaves (Figure 7) [91]. Furthermore, PSI-PI treatment represses Fe-deficiency genes, whereas HL has no effect on the expression of these genes (Figure S6) [62]. Importantly, the PSI-PI treatment also clearly induces the genes encoding sinks for electrons from PSI, whereas the expression of these genes was not specifically altered under HL [62,102].

5. Conclusions

Taken together (Figure 8), we conclude that PSI photoinhibition results in damage to FeS clusters and the subsequent release of Fe from PSI. Excessive-Fe stress in the chloroplast initiates a novel retrograde signal to modify nuclear gene expression. Such a signaling cascade controls the expression of iron homeostasis genes and probably also affects the expression of CEF components, the CBB cycle, and photorespiration genes. These changes in nuclear gene expression help plants to survive both the actual stress and subsequent recovery periods.

It was also shown that CO₂ deprivation activates genes involved in the biosynthesis of flavonoids via the JA/OPDA signaling cascade. Flavonoids are known to alleviate oxidative stress that is induced in the absence of CO₂ in plant leaves.

Supplementary Materials: The following supporting information can be downloaded at <https://www.mdpi.com/article/10.3390/antiox12111902/s1>: Figure S1. Stomatal aperture in control plant leaves and in leaves treated with PSI photoinhibition light regime for three hours. Figure S2. The number of differentially expressed genes (DEGs) in both control (GL) and PSI-PI-treated plants at indicated CO₂ concentrations. Figure S3. Localization of the enzymes in Calvin–Benson–Bassham (CBB) cycle and photorespiration pathway in leaves exposed to PSI photoinhibition. Figure S4. Differential expression of genes involved in starch and sucrose metabolism in *Arabidopsis*. Figure S5. Differential expression of NO-responsive genes in leaves exposed to PSI photoinhibition at various CO₂ concentrations. Figure S6. Comparison of the gene expression in plants exposed to PSI photoinhibition treatment (PSI-PI) with that in plants exposed to high-light (HL) treatment. Figure S7. Differential expression (log₂ values) of *Arabidopsis* nuclear genes encoding (A) photosynthetic electron transport chain (PETC) components, including cyclic electron flow (CEF) components, and (B) Calvin–Benson–Bassham (CBB) cycle and photorespiratory components in leaves exposed to chemical or environmental treatments indicated above the columns. Table S1. Differentially expressed genes in *Arabidopsis thaliana* leaves treated with either growth light (GL) or with PSI photoinhibition light regime (PSI-PI) at various CO₂ concentrations. Table S2. Significantly enriched Gene Ontology (GO) terms among the differentially expressed genes (DEGs) in leaves illuminated under growth light (GL) or with PSI photoinhibition light regime (PSI-PI) at various CO₂ concentrations. Table S3. The lists of nuclear genes used to construct the heatmaps presented in the article. References [33,60–62,107] are cited in the supplementary materials.

Author Contributions: Conceptualization, M.K., V.K., P.J.G., E.-M.A. and E.R.; methodology, M.K., V.K. and P.J.G.; investigation, M.K. and V.K.; writing—original draft preparation, M.K. and E.R.; writing—review and editing, M.K., P.J.G., E.-M.A. and E.R.; funding acquisition; E.-M.A. and E.R. All authors have read and agreed to the published version of the manuscript.

Funding: This research was funded by the Jane and Aatos Erkkö Foundation.

Institutional Review Board Statement: Not applicable.

Data Availability Statement: Raw data files and count datasets generated for this study are stored in NCBI's Gene Expression Omnibus (GEO) with the accession code GSE242125.

Acknowledgments: Mika Keränen is thanked for excellent technical assistance.

Conflicts of Interest: The authors declare no conflict of interest.

References

1. Dietz, K.J.; Turkan, I.; Krieger-Liszak, A. Redox- and reactive oxygen species-dependent signaling into and out of the photosynthesizing chloroplast. *Plant Physiol.* **2016**, *171*, 1541–1550. [[CrossRef](#)] [[PubMed](#)]
2. Foyer, C.H.; Hanke, G. ROS production and signalling in chloroplasts: Cornerstones and evolving concepts. *Plant J.* **2022**, *111*, 642–661. [[CrossRef](#)]
3. Aro, E.M.; Virgin, I.; Andersson, B. Photoinhibition of photosystem II. Inactivation, protein damage and turnover. *Biochim. Biophys. Acta* **1993**, *1143*, 113–134. [[CrossRef](#)]
4. Tikkanen, M.; Mekala, N.R.; Aro, E.M. Photosystem II photoinhibition-repair cycle protects photosystem I from irreversible damage. *Biochim. Biophys. Acta* **2014**, *1837*, 210–215. [[CrossRef](#)] [[PubMed](#)]
5. Havaux, M.; Davaud, A. Photoinhibition of photosynthesis in chilled potato leaves is not correlated with a loss of photosystem II activity: Preferential inactivation of photosystem I. *Photosynth. Res.* **1994**, *40*, 75–92. [[CrossRef](#)] [[PubMed](#)]
6. Zhang, S.; Scheller, H.V. Photoinhibition of photosystem I at chilling temperature and subsequent recovery in *Arabidopsis thaliana*. *Plant Cell Physiol.* **2004**, *45*, 1595–1602. [[CrossRef](#)]
7. Kudoh, H.; Sonoike, K. Irreversible damage to photosystem I by chilling in the light: Cause of the degradation of chlorophyll after returning to normal growth temperature. *Planta* **2002**, *215*, 541–548. [[CrossRef](#)]
8. Sonoike, K. Photoinhibition of photosystem I. *Physiol. Plant.* **2011**, *142*, 56–64. [[CrossRef](#)]
9. Sonoike, K.; Kamo, M.; Hihara, Y.; Hiyama, T.; Enami, I. The mechanism of the degradation of PsaB gene product, one of the photosynthetic reaction center subunits of photosystem I, upon photoinhibition. *Photosynth. Res.* **1997**, *53*, 55–63. [[CrossRef](#)]
10. Khorobrykh, S.; Havurinne, V.; Mattila, H.; Tyystjärvi, E. Oxygen and ROS in photosynthesis. *Plants* **2020**, *9*, 91. [[CrossRef](#)]
11. Takagi, D.; Takumi, S.; Hashiguchi, M.; Sejima, T.; Miyake, C. Superoxide and singlet oxygen produced within the thylakoid membranes both cause photosystem I photoinhibition. *Plant Physiol.* **2016**, *171*, 1626–1634. [[CrossRef](#)] [[PubMed](#)]
12. Tiwari, A.; Mamedov, F.; Grieco, M.; Suorsa, M.; Jajoo, A.; Styring, S.; Tikkanen, M.; Aro, E.M. Photodamage of iron-sulphur clusters in photosystem I induces non-photochemical energy dissipation. *Nat. Plants* **2016**, *2*, 16035. [[CrossRef](#)]
13. Sonoike, K. photoinhibition of photosystem I: Its physiological significance in the chilling sensitivity of plants. *Plant Cell Physiol.* **1996**, *37*, 239–247. [[CrossRef](#)]
14. Tjus, S.E.; Møller, B.L.; Scheller, H.V. Photoinhibition of photosystem I damages both reaction centre proteins PSI-A and PSI-B and acceptor-side located small photosystem I polypeptides. *Photosynth. Res.* **1999**, *60*, 75–86. [[CrossRef](#)]
15. Hernández-Verdeja, T.; Strand, Å. Retrograde signals navigate the path to chloroplast development. *Plant Physiol.* **2018**, *176*, 967–976. [[CrossRef](#)] [[PubMed](#)]
16. Richter, A.S.; Nägele, T.; Grimm, B.; Kaufmann, K.; Schroda, M.; Leister, D.; Kleine, T. Retrograde signaling in plants: A critical review focusing on the GUN pathway and beyond. *Plant Commun.* **2023**, *4*, 100511. [[CrossRef](#)]
17. Jan, M.; Liu, Z.; Rochaix, J.D.; Sun, X. Retrograde and anterograde signaling in the crosstalk between chloroplast and nucleus. *Front. Plant Sci.* **2022**, *13*, 980237. [[CrossRef](#)]
18. Singh, R.; Singh, S.; Parihar, P.; Singh, V.P.; Prasad, S.M. Retrograde signaling between plastid and nucleus: A review. *Plant Physiol.* **2015**, *181*, 55–66. [[CrossRef](#)]
19. Park, S.W.; Li, W.; Viehhauser, A.; He, B.; Kim, S.; Nilsson, A.K.; Andersson, M.X.; Kittle, J.D.; Ambavaram, M.M.R.; Luan, S.; et al. Cyclophilin 20-3 relays a 12-oxo-phytyldienoic acid signal during stress responsive regulation of cellular redox homeostasis. *Proc. Natl. Acad. Sci. USA* **2013**, *110*, 9559–9564. [[CrossRef](#)]
20. Stintzi, A.; Weber, H.; Reymond, P.; Browse, J.; Farmer, E.E. Plant defense in the absence of jasmonic acid: The role of cyclopentenones. *Proc. Natl. Acad. Sci. USA* **2001**, *98*, 12837–12842. [[CrossRef](#)]
21. Liu, W.; Park, S.W. 12-oxo-phytyldienoic acid: A fuse and/or switch of plant growth and defense responses? *Front. Plant Sci.* **2021**, *12*, 1687. [[CrossRef](#)] [[PubMed](#)]
22. Gollan, P.J.; Aro, E.M. Photosynthetic signalling during high light stress and recovery: Targets and dynamics. *Philos. Trans. R. Soc. Lond. B Biol. Sci.* **2020**, *375*, 20190406. [[CrossRef](#)] [[PubMed](#)]
23. Shan, X.; Zhang, Y.; Peng, W.; Wang, Z.; Xie, D. Molecular mechanism for jasmonate-induction of anthocyanin accumulation in *Arabidopsis*. *J. Exp. Bot.* **2009**, *60*, 3849–3860. [[CrossRef](#)]
24. Lima-Melo, Y.; Kılıç, M.; Aro, E.M.; Gollan, P.J. Photosystem I inhibition, protection and signalling: Knowns and unknowns. *Front. Plant Sci.* **2021**, *12*, 791124. [[CrossRef](#)] [[PubMed](#)]
25. Tikkanen, M.; Grebe, S. Switching off Photoprotection of photosystem I—A novel tool for gradual PSI photoinhibition. *Physiol. Plant.* **2018**, *162*, 156–161. [[CrossRef](#)]
26. Kramer, D.M.; Johnson, G.; Kiirats, O.; Edwards, G.E. New fluorescence parameters for the determination of QA redox state and excitation energy fluxes. *Photosynth. Res.* **2004**, *79*, 209–218. [[CrossRef](#)] [[PubMed](#)]
27. Oxborough, K.; Baker, N.R. Resolving chlorophyll a fluorescence images of photosynthetic efficiency into photochemical and non-photochemical components—Calculation of QP and Fv'/Fm' without measuring Fo'. *Photosynth. Res.* **1997**, *54*, 135–142. [[CrossRef](#)]
28. Lempiäinen, T.; Rintamäki, E.; Aro, E.M.; Tikkanen, M. Plants acclimate to photosystem I photoinhibition by readjusting the photosynthetic machinery. *Plant Cell Environ.* **2022**, *45*, 2954–2971. [[CrossRef](#)]
29. Genty, B.; Briantais, J.M.; Baker, N.R. The relationship between the quantum yield of photosynthetic electron transport and quenching of chlorophyll fluorescence. *Biochim. Biophys. Acta* **1989**, *990*, 87–92. [[CrossRef](#)]

30. Patro, R.; Duggal, G.; Love, M.I.; Irizarry, R.A.; Kingsford, C. Salmon provides fast and bias-aware quantification of transcript expression. *Nat. Methods* **2017**, *14*, 417–419. [[CrossRef](#)]
31. Sonesson, C.; Love, M.I.; Robinson, M.D. Differential analyses for RNA-Seq: Transcript-level estimates improve gene-level inferences. *F1000Research* **2015**, *4*, 1521. [[CrossRef](#)] [[PubMed](#)]
32. Love, M.I.; Huber, W.; Anders, S. Moderated estimation of fold change and dispersion for rna-seq data with DESeq2. *Genome Biol.* **2014**, *15*, 550. [[CrossRef](#)] [[PubMed](#)]
33. Ashburner, M.; Ball, C.A.; Blake, J.A.; Botstein, D.; Butler, H.; Cherry, J.M.; Davis, A.P.; Dolinski, K.; Dwight, S.S.; Eppig, J.T.; et al. Gene ontology: Tool for the unification of biology. *Nat. Genet.* **2000**, *25*, 25–29. [[CrossRef](#)]
34. Consortium, T.G.O.; Aleksander, S.A.; Balhoff, J.; Carbon, S.; Cherry, J.M.; Drabkin, H.J.; Ebert, D.; Feuermann, M.; Gaudet, P.; Harris, N.L.; et al. The gene ontology knowledgebase in 2023. *Genetics* **2023**, *224*, iyad031. [[CrossRef](#)] [[PubMed](#)]
35. Thomas, P.D.; Ebert, D.; Muruganujan, A.; Mushayahama, T.; Albou, L.P.; Mi, H. PANTHER: Making genome-scale phylogenetics accessible to all. *Protein Sci.* **2022**, *31*, 8–22. [[CrossRef](#)]
36. Xu, Z.; Jiang, Y.; Jia, B.; Zhou, G. Elevated-CO₂ response of stomata and its dependence on environmental factors. *Front. Plant Sci.* **2016**, *7*, 657. [[CrossRef](#)] [[PubMed](#)]
37. Liu, H.; Liu, Z.; Wu, Y.; Zheng, L.; Zhang, G. Regulatory mechanisms of anthocyanin biosynthesis in apple and pear. *Int. J. Mol. Sci.* **2021**, *22*, 8441. [[CrossRef](#)]
38. Dao, T.T.H.; Linthorst, H.J.M.; Verpoorte, R. Chalcone synthase and its functions in plant resistance. *Phytochem. Rev.* **2011**, *10*, 397–412. [[CrossRef](#)] [[PubMed](#)]
39. Lin, Y.; Laosatit, K.; Liu, J.; Chen, J.; Yuan, X.; Somta, P.; Chen, X. The mungbean VrP locus encoding MYB90, an R2R3-Type MYB protein, regulates anthocyanin biosynthesis. *Front. Plant Sci.* **2022**, *13*, 895634. [[CrossRef](#)]
40. Yan, H.; Pei, X.; Zhang, H.; Li, X.; Zhang, X.; Zhao, M.; Chiang, V.L.; Sederoff, R.R.; Zhao, X. MYB-mediated regulation of anthocyanin biosynthesis. *Int. J. Mol. Sci.* **2021**, *22*, 3103. [[CrossRef](#)]
41. Briat, J.F.; Duc, C.; Ravet, K.; Gaymard, F. Ferritins and iron storage in plants. *Biochim. Biophys. Acta* **2010**, *1800*, 806–814. [[CrossRef](#)] [[PubMed](#)]
42. Tissot, N.; Robe, K.; Gao, F.; Grant-Grant, S.; Boucherez, J.; Bellegarde, F.; Maghiaoui, A.; Marcelin, R.; Izquierdo, E.; Benhamed, M.; et al. Transcriptional integration of the responses to iron availability in *Arabidopsis* by the BHLH factor ILR3. *New Phytol.* **2019**, *223*, 1433–1446. [[CrossRef](#)] [[PubMed](#)]
43. Mukherjee, I.; Campbell, N.H.; Ash, J.S.; Connolly, E.L. Expression profiling of the *Arabidopsis* ferric chelate reductase (FRO) gene family reveals differential regulation by iron and copper. *Planta* **2006**, *223*, 1178–1190. [[CrossRef](#)] [[PubMed](#)]
44. Sági-Kazár, M.; Solymosi, K.; Solti, Á. Iron in leaves: Chemical forms, signalling, and in-cell distribution. *J. Exp. Bot.* **2022**, *73*, 1717–1734. [[CrossRef](#)] [[PubMed](#)]
45. Takahashi, S.; Ogawa, T.; Inoue, K.; Masuda, T. Characterization of cytosolic tetrapyrrole-binding proteins in *Arabidopsis thaliana*. *Photochem. Photobiol. Sci.* **2008**, *7*, 1216–1224. [[CrossRef](#)] [[PubMed](#)]
46. Hsieh, E.J.; Lin, W.D.; Schmidt, W. Genomically hardwired regulation of gene activity orchestrates cellular iron homeostasis in *Arabidopsis*. *RNA Biol.* **2022**, *19*, 143–161. [[CrossRef](#)]
47. Pan, I.C.; Tsai, H.H.; Cheng, Y.T.; Wen, T.N.; Buckhout, T.J.; Schmidt, W. Post-transcriptional coordination of the *Arabidopsis* iron deficiency response is partially dependent on the E3 ligase ring domain ligase 1 (RGLG1) and ring domain ligase 2 (RGLG2). *Mol. Cell. Proteom.* **2015**, *14*, 2733–2752. [[CrossRef](#)]
48. Gangappa, S.N.; Botto, J.F. The multifaceted roles of HY5 in plant growth and development. *Mol. Plant* **2016**, *9*, 1353–1365. [[CrossRef](#)]
49. Xiao, Y.; Chu, L.; Zhang, Y.; Bian, Y.; Xiao, J.; Xu, D. HY5: A pivotal regulator of light-dependent development in higher plants. *Front. Plant Sci.* **2022**, *12*, 800989. [[CrossRef](#)]
50. Holm, M.; Ma, L.G.; Qu, L.J.; Deng, X.W. Two interacting BZIP proteins are direct targets of COP1-mediated control of light-dependent gene expression in *Arabidopsis*. *Genes Dev.* **2002**, *16*, 1247–1259. [[CrossRef](#)]
51. Harmon, F.G.; Kay, S.A. The F Box protein AFR is a positive regulator of phytochrome a-mediated light signaling. *Curr. Biol.* **2003**, *13*, 2091–2096. [[CrossRef](#)] [[PubMed](#)]
52. Liu, C.; Zhang, Q.; Zhu, H.; Cai, C.; Li, S. Characterization of mungbean constans-like genes and functional analysis of constans-like 2 in the regulation of flowering time in *Arabidopsis*. *Front. Plant Sci.* **2021**, *12*, 608603. [[CrossRef](#)] [[PubMed](#)]
53. Mellenthin, M.; Ellersiek, U.; Börger, A.; Baier, M. Expression of the *Arabidopsis* sigma factor SIG5 is photoreceptor and photosynthesis controlled. *Plants* **2014**, *3*, 359–391. [[CrossRef](#)]
54. Ma, M.; Liu, Y.; Bai, C.; Yong, J.W.H. The Significance of chloroplast NAD(P)H dehydrogenase complex and its dependent cyclic electron transport in photosynthesis. *Front. Plant Sci.* **2021**, *12*, 661863. [[CrossRef](#)] [[PubMed](#)]
55. Munekage, Y.; Hojo, M.; Meurer, J.; Endo, T.; Tasaka, M.; Shikanai, T. PGR5 is involved in cyclic electron flow around photosystem I and is essential for photoprotection in *Arabidopsis*. *Cell* **2002**, *110*, 361–371. [[CrossRef](#)]
56. Shikanai, T.; Endo, T.; Hashimoto, T.; Yamada, Y.; Asada, K.; Yokota, A. Directed disruption of the tobacco NdhB gene impairs cyclic electron flow around photosystem I. *Proc. Natl. Acad. Sci. USA* **1998**, *95*, 9705–9709. [[CrossRef](#)]
57. Suorsa, M.; Rossi, F.; Tadini, L.; Labs, M.; Colombo, M.; Jahns, P.; Kater, M.M.M.; Leister, D.; Finazzi, G.; Aro, E.M.; et al. PGR5-PGRL1-dependent cyclic electron transport modulates linear electron transport rate in *Arabidopsis thaliana*. *Mol. Plant* **2016**, *9*, 271–288. [[CrossRef](#)]

58. Khozaei, M.; Fisk, S.; Lawson, T.; Gibon, Y.; Sulpice, R.; Stitt, M.; Lefebvre, S.C.; Raines, C.A. Overexpression of plastid transketolase in tobacco results in a thiamine auxotrophic phenotype. *Plant Cell* **2015**, *27*, 432–447. [[CrossRef](#)]
59. Laxa, M.; Fromm, S. Co-expression and regulation of photorespiratory genes in *Arabidopsis thaliana*: A bioinformatic approach. *Curr. Plant Biol.* **2018**, *14*, 2–18. [[CrossRef](#)]
60. Parani, M.; Rudrabhatla, S.; Myers, R.; Weirich, H.; Smith, B.; Leaman, D.W.; Goldman, S.L. Microarray analysis of nitric oxide responsive transcripts in *Arabidopsis*. *Plant Biotechnol. J.* **2004**, *2*, 359–366. [[CrossRef](#)] [[PubMed](#)]
61. Polverari, A.; Molesini, B.; Pezzotti, M.; Buonauro, R.; Marte, M.; Delledonne, M. Nitric oxide-mediated transcriptional changes in *Arabidopsis thaliana*. *Mol. Plant-Microbe Interact* **2003**, *16*, 1094–1105. [[CrossRef](#)] [[PubMed](#)]
62. Alvarez-Fernandez, R.; Penfold, C.A.; Galvez-Valdivieso, G.; Exposito-Rodriguez, M.; Stallard, E.J.; Bowden, L.; Moore, J.D.; Mead, A.; Davey, P.A.; Matthews, J.S.A.; et al. Time-Series transcriptomics reveals a BBX32-directed control of acclimation to high light in mature *Arabidopsis* leaves. *Plant J.* **2021**, *107*, 1363–1386. [[CrossRef](#)] [[PubMed](#)]
63. Hruz, T.; Laule, O.; Szabo, G.; Wessendorp, F.; Bleuler, S.; Oertle, L.; Widmayer, P.; Gruissem, W.; Zimmermann, P. Genevestigator v3: A reference expression database for the meta-analysis of transcriptomes. *Adv. Bioinform.* **2008**, *2008*, 420747. [[CrossRef](#)] [[PubMed](#)]
64. Op Den Camp, R.G.L.; Przybyla, D.; Ochsenbein, C.; Lalo, C.; Kim, C.; Danon, A.; Wagner, D.; Hideg, É.; Göbel, C.; Feussner, I.; et al. Rapid induction of distinct stress responses after the release of singlet oxygen in *Arabidopsis*. *Plant Cell* **2003**, *15*, 2320–2332. [[CrossRef](#)]
65. Lima-Melo, Y.; Gollan, P.J.; Tikkanen, M.; Silveira, J.A.G.; Aro, E.M. Consequences of photosystem-I damage and repair on photosynthesis and carbon use in *Arabidopsis thaliana*. *Plant J.* **2019**, *97*, 1061–1072. [[CrossRef](#)] [[PubMed](#)]
66. Sonoike, K.; Terashima, I.; Iwaki, M.; Itoh, S. Destruction of photosystem I iron-sulfur centers in leaves of *Cucumis Sativus* L. by weak illumination at chilling temperatures. *FEBS Lett.* **1995**, *362*, 235–238. [[CrossRef](#)]
67. Hendriks, J.H.M.; Kolbe, A.; Gibon, Y.; Stitt, M.; Geigenberger, P. ADP-glucose pyrophosphorylase is activated by posttranslational redox-modification in response to light and to sugars in leaves of *Arabidopsis* and other plant species. *Plant Physiol.* **2003**, *133*, 838–849. [[CrossRef](#)]
68. Michalska, J.; Zaubner, H.; Buchanan, B.B.; Cejudo, F.J.; Geigenberger, P. NTRC links built-in thioredoxin to light and sucrose in regulating starch synthesis in chloroplasts and amyloplasts. *Proc. Natl. Acad. Sci. USA* **2009**, *106*, 9908–9913. [[CrossRef](#)]
69. Wiese, A.; Christ, M.M.; Virnich, O.; Schurr, U.; Walter, A. Spatio-temporal leaf growth patterns of *Arabidopsis thaliana* and evidence for sugar control of the diel leaf growth cycle. *New Phytol.* **2007**, *174*, 752–761. [[CrossRef](#)]
70. Gibon, Y.; Pyl, E.T.; Sulpice, R.; Lunn, J.E.; HÖhne, M.; Günther, M.; Stitt, M. Adjustment of growth, starch turnover, protein content and central metabolism to a decrease of the carbon supply when *Arabidopsis* is grown in very short photoperiods. *Plant Cell Environ.* **2009**, *32*, 859–874. [[CrossRef](#)]
71. MacNeill, G.J.; Mehrpouyan, S.; Minow, M.A.A.; Patterson, J.A.; Tetlow, I.J.; Emes, M.J. Starch as a source, starch as a sink: The bifunctional role of starch in carbon allocation. *J. Exp. Bot.* **2017**, *68*, 4433–4453. [[CrossRef](#)] [[PubMed](#)]
72. Sulpice, R.; Pyl, E.T.; Ishihara, H.; Trenkamp, S.; Steinfath, M.; Witucka-Wall, H.; Gibon, Y.; Usadel, B.; Poree, F.; Piques, M.C.; et al. Starch as a major integrator in the regulation of plant growth. *Proc. Natl. Acad. Sci. USA* **2009**, *106*, 10348–10353. [[CrossRef](#)] [[PubMed](#)]
73. Mierziak, J.; Kostyn, K.; Kulma, A. Flavonoids as important molecules of plant interactions with the environment. *Molecules* **2014**, *19*, 16240–16265. [[CrossRef](#)] [[PubMed](#)]
74. Banerjee, S.; Siemianowski, O.; Liu, M.; Lind, K.R.; Tian, X.; Nettleton, D.; Cademartiri, L. Stress response to CO₂ deprivation by *Arabidopsis thaliana* in plant cultures. *PLoS ONE* **2019**, *14*, e0212462. [[CrossRef](#)] [[PubMed](#)]
75. Gou, J.Y.; Felippes, F.F.; Liu, C.J.; Weigel, D.; Wang, J.W. Negative regulation of anthocyanin biosynthesis in *Arabidopsis* by a MiR156-targeted SPL transcription factor. *Plant Cell* **2011**, *23*, 1512–1522. [[CrossRef](#)] [[PubMed](#)]
76. Zhou, H.; Lin-Wang, K.; Liao, L.; Gu, C.; Lu, Z.; Allan, A.C.; Han, Y. Peach MYB7 activates transcription of the proanthocyanidin pathway gene encoding leucoanthocyanidin reductase, but not anthocyanidin reductase. *Front. Plant Sci.* **2015**, *6*, 908. [[CrossRef](#)]
77. Borevitz, J.O.; Xia, Y.; Blount, J.; Dixon, R.A.; Lamb, C. Activation tagging identifies a conserved MYB regulator of phenylpropanoid biosynthesis. *Plant Cell* **2000**, *12*, 2383–2393. [[CrossRef](#)]
78. Gonzalez, A.; Zhao, M.; Leavitt, J.M.; Lloyd, A.M. Regulation of the anthocyanin biosynthetic pathway by the TTG1/BHLH/Myb transcriptional complex in *Arabidopsis* seedlings. *Plant J.* **2008**, *53*, 814–827. [[CrossRef](#)]
79. Qi, T.; Song, S.; Ren, Q.; Wu, D.; Huang, H.; Chen, Y.; Fan, M.; Peng, W.; Ren, C.; Xie, D. The jasmonate-ZIM-domain proteins interact with the WD-repeat/BHLH/MYB complexes to regulate jasmonate-mediated anthocyanin accumulation and trichome initiation in *Arabidopsis thaliana*. *Plant Cell* **2011**, *23*, 1795–1814. [[CrossRef](#)]
80. Zhou, M.; Memelink, J. Jasmonate-responsive transcription factors regulating plant secondary metabolism. *Biotechnol. Adv.* **2016**, *34*, 441–449. [[CrossRef](#)]
81. Ochsenbein, C.; Przybyla, D.; Danon, A.; Landgraf, F.; Göbel, C.; Imboden, A.; Feussner, I.; Apel, K. The role of EDS1 (enhanced disease susceptibility) during singlet oxygen-mediated stress responses of *Arabidopsis*. *Plant J.* **2006**, *47*, 445–456. [[CrossRef](#)] [[PubMed](#)]
82. Przybyla, D.; Göbel, C.; Imboden, A.; Hamberg, M.; Feussner, I.; Apel, K. Enzymatic, but not non-enzymatic, ¹O₂-mediated peroxidation of polyunsaturated fatty acids forms part of the EXECUTER1-dependent stress response program in the Flu mutant of *Arabidopsis thaliana*. *Plant J.* **2008**, *54*, 236–248. [[CrossRef](#)]
83. Jeong, J.; Cohe, C.; Kerkeb, L.; Pilon, M.; Connolly, E.L.; Guerinot, M. Lou Chloroplast Fe(III) chelate reductase activity is essential for seedling viability under iron limiting conditions. *Proc. Natl. Acad. Sci. USA* **2008**, *105*, 10619–10624. [[CrossRef](#)] [[PubMed](#)]

84. Nechushtai, R.; Karmi, O.; Zuo, K.; Marjault, H.B.; Darash-Yahana, M.; Sohn, Y.S.; King, S.D.; Zandalinas, S.I.; Carloni, P.; Mittler, R. The balancing act of NEET proteins: Iron, ROS, calcium and metabolism. *Biochim. Biophys. Acta* **2020**, *1867*, 118805. [[CrossRef](#)] [[PubMed](#)]
85. Ravet, K.; Touraine, B.; Boucherez, J.; Briat, J.F.; Gaymard, F.; Cellier, F. Ferritins control interaction between iron homeostasis and oxidative stress in *Arabidopsis*. *Plant J.* **2009**, *57*, 400–412. [[CrossRef](#)]
86. Bauer, P.; Ling, H.Q.; Guerinot, M. Lou FIT, the FER-like iron deficiency induced transcription factor in *Arabidopsis*. *Plant Physiol. Biochem.* **2007**, *45*, 260–261. [[CrossRef](#)]
87. Okada, S.; Lei, G.J.; Yamaji, N.; Huang, S.; Ma, J.F.; Mochida, K.; Hirayama, T. FE uptake-inducing peptide 1 maintains Fe translocation by controlling Fe deficiency response genes in the vascular tissue of *Arabidopsis*. *Plant Cell Environ.* **2022**, *45*, 3322–3337. [[CrossRef](#)]
88. Sivitz, A.B.; Hermand, V.; Curie, C.; Vert, G. Arabidopsis BHLH100 and BHLH101 control iron homeostasis via a FIT-independent pathway. *PLoS ONE* **2012**, *7*, e44843. [[CrossRef](#)]
89. Busch, A.; Rimbauld, B.; Naumann, B.; Rensch, S.; Hippler, M. Ferritin is required for rapid remodeling of the photosynthetic apparatus and minimizes photo-oxidative stress in response to iron availability in *Chlamydomonas reinhardtii*. *Plant J.* **2008**, *55*, 201–211. [[CrossRef](#)]
90. Lima-Melo, Y.; Alencar, V.T.C.B.; Lobo, A.K.M.; Sousa, R.H.V.; Tikkanen, M.; Aro, E.-M.; Silveira, J.A.G.; Gollan, P.J. Photoinhibition of photosystem I provides oxidative protection during imbalanced photosynthetic electron transport in *Arabidopsis thaliana*. *Front. Plant Sci.* **2019**, *10*, 916. [[CrossRef](#)]
91. Gollan, P.J.; Lima-Melo, Y.; Tiwari, A.; Tikkanen, M.; Aro, E.M. Interaction between photosynthetic electron transport and chloroplast sinks triggers protection and signalling important for plant productivity. *Philos. Trans. R. Soc. Lond. B Biol. Sci.* **2017**, *372*, 20160390. [[CrossRef](#)] [[PubMed](#)]
92. Zhang, C.; Wu, Y.; Liu, X.; Zhang, J.; Li, X.; Lin, L.; Yin, R. Pivotal roles of elongated hypocotyl 5 in regulation of plant development and fruit metabolism in tomato. *Plant Physiol.* **2022**, *189*, 527–540. [[CrossRef](#)] [[PubMed](#)]
93. Jiang, X.; Xu, J.; Lin, R.; Song, J.; Shao, S.; Yu, J.; Zhou, Y. Light-induced HY5 functions as a systemic signal to coordinate the photoprotective response to light fluctuation. *Plant Physiol.* **2020**, *184*, 1181–1193. [[CrossRef](#)] [[PubMed](#)]
94. Brown, B.A.; Jenkins, G.I. UV-B Signaling pathways with different fluence-rate response profiles are distinguished in mature *Arabidopsis* leaf tissue by requirement for UVR8, HY5, and HYH. *Plant Physiol.* **2008**, *146*, 576–588. [[CrossRef](#)]
95. Cackett, L.; Luginbuehl, L.H.; Schreier, T.B.; Lopez-Juez, E.; Hibberd, J.M. Chloroplast development in green plant tissues: The interplay between light, hormone, and transcriptional regulation. *New Phytol.* **2022**, *233*, 2000–2016. [[CrossRef](#)]
96. Lepistö, A.; Rintamäki, E. Coordination of plastid and light signaling pathways upon development of *Arabidopsis* leaves under various photoperiods. *Mol. Plant* **2012**, *5*, 799–816. [[CrossRef](#)]
97. Ruckle, M.E.; Larkin, R.M. Plastid signals that affect photomorphogenesis in *Arabidopsis thaliana* are dependent on genomes uncoupled 1 and cryptochrome 1. *New Phytol.* **2009**, *182*, 367–379. [[CrossRef](#)]
98. Nagashima, A.; Hanaoka, M.; Shikanai, T.; Fujiwara, M.; Kanamaru, K.; Takahashi, H.; Tanaka, K. The multiple-stress responsive plastid sigma factor, SIG5, directs activation of the PsbD blue light-responsive promoter (BLRP) in *Arabidopsis thaliana*. *Plant Cell Physiol.* **2004**, *45*, 357–368. [[CrossRef](#)]
99. Legen, J.; Kemp, S.; Krause, K.; Profanter, B.; Herrmann, R.G.; Maier, R.M. Comparative analysis of plastid transcription profiles of entire plastid chromosomes from tobacco attributed to wild-type and PEP-deficient transcription machineries. *Plant J.* **2002**, *31*, 171–188. [[CrossRef](#)]
100. Waters, M.T.; Wang, P.; Korkaric, M.; Capper, R.G.; Saunders, N.J.; Langdale, J.A. GLK Transcription factors coordinate expression of the photosynthetic apparatus in *Arabidopsis*. *Plant Cell* **2009**, *21*, 1109–1128. [[CrossRef](#)]
101. Kim, N.; Jeong, J.; Kim, J.; Oh, J.; Choi, G. Shade represses photosynthetic genes by disrupting the DNA binding of golden2-like1. *Plant Physiol.* **2023**, *191*, 2334–2352. [[CrossRef](#)] [[PubMed](#)]
102. Huang, J.; Zhao, X.; Correspondence, J.C.; Chory, J. The *Arabidopsis* transcriptome responds specifically and dynamically to high light stress. *Cell Rep.* **2019**, *29*, 4186–4199. [[CrossRef](#)] [[PubMed](#)]
103. Fitzpatrick, D.; Aro, E.M.; Tiwari, A. True oxygen reduction capacity during photosynthetic electron transfer in thylakoids and intact leaves. *Plant Physiol.* **2022**, *189*, 112–128. [[CrossRef](#)] [[PubMed](#)]
104. Farmer, E.E.; Mueller, M.J. ROS-mediated lipid peroxidation and RES-activated signaling. *Annu. Rev. Plant Biol.* **2013**, *64*, 429–450. [[CrossRef](#)]
105. Murata, N.; Takahashi, S.; Nishiyama, Y.; Allakhverdiev, S.I. Photoinhibition of photosystem II under environmental stress. *Biochim. Biophys. Acta* **2007**, *1767*, 414–421. [[CrossRef](#)]
106. Tyystjärvi, E.; Aro, E.M. The rate constant of photoinhibition, measured in lincomycin-treated leaves, is directly proportional to light intensity. *Proc. Natl. Acad. Sci. USA* **1996**, *93*, 2213–2218. [[CrossRef](#)]
107. Mi, H.; Muruganujan, A.; Ebert, D.; Huang, X.; Thomas, P.D. PANTHER version 14: More genomes, a new PANTHER GO-slim and improvements in enrichment analysis tools. *Nucleic Acids Res.* **2019**, *47*, D419–D426. [[CrossRef](#)]

Disclaimer/Publisher’s Note: The statements, opinions and data contained in all publications are solely those of the individual author(s) and contributor(s) and not of MDPI and/or the editor(s). MDPI and/or the editor(s) disclaim responsibility for any injury to people or property resulting from any ideas, methods, instructions or products referred to in the content.